An-Najah National University

Faculty of Graduate Studies

POLYMER WITH A DUAL ADSORPTION SITES: DESIGN, SYNTHESIS AND PURIFICATION OF POLLUTED WTAER FROM HEAVY METALS AND TOXIC ANIONS

By

Raneem Ahmad Abu Aysheh

Supervisor

Prof. Othman Hamed

This Thesis is Submitted in Partial Fulfillment of the Requirements for the Degree of Master of Chemistry, Faculty of Graduate Studies, An-Najah National University, Nablus - Palestine.

2023

POLYMER WITH A DUAL ADSORPTION SITES: DESIGN, SYNTHESIS AND PURIFICATION OF POLLUTED WTAER FROM HEAVY METALS AND TOXIC ANIONS

By

Raneem Ahmad Abu Aysheh

This thesis was successfully defended on 3/ 4 /2023 and approved by

Defense Committee Members	**Signature**
Prof. Othman Hamed / Supervisor	**……**
Dr. Abdalhadi Deghles / Internal Examiner	**……**
Dr. Derar Smadi / External Examiner	**……**

Dedication

To my loving dad and mom who support me to be the person that I always dreamed of. wishing them both long lives and good health.

To my lovely husband, thank you for your greatest support.

For my whole family.

To my close friends who have supported me through every step of my life.

I also dedicate this work to my creative doctors and professors who never failed to supply me with crucial information during my studies.

To everyone who was in my life and is still doing so, I am grateful for your love and support.

Acknowledgment

The biggest and greatest thanks be to Allah, the Most Merciful, who led and guided me along the right way.

I would particularly like to thank Professor Othman Hamed, who is my research supervisor, for allowing me to work with him. And for his direction and advice in obtaining quality research and good results. Additionally, I'd like to thank all of the professors and doctors who helped me earn my master's degree.

I also appreciate my colleagues and friends especially, Angham, Reem, Jomana, Haneen and I am grateful for the days that brought us together. Finally, I would like to thank to Mr. Ameed Amireh, my supervisor in the chemistry lab, and all lab technicians at An-Najah National University, for his assistance and support during this work.

Declaration

I, the undersigned, declare that I submitted the thesis entitled:

POLYMER WITH A DUAL ADSORPTION SITES: DESIGN, SYNTHESIS AND PURIFICATION OF POLLUTED WTAER FROM HEAVY METALS AND TOXIC ANIONS

I declare that the work provided in this thesis, unless otherwise referenced, is the researcher's own work, and has not been submitted elsewhere for any other degree or qualification.

Student's Name: _____

Signature: _____

Date: _____

List of Contents

List of Tables

List of Figures

List of Schemes

List of Appendices

POLYMER WITH A DUAL ADSORPTION SITES: DESIGN, SYNTHESIS AND PURIFICATION OF POLLUTED WTAER FROM HEAVY METALS AND TOXIC ANIONS

By
Raneem Ahmad Abu Aysheh
Supervisor
Prof. Othman Hamed

Abstract

Demand for clean is increasing due to the increase in population. Recycling of contaminated wastewater could be an answer for this issue. Wastewater is contaminated with a variety of toxic materials depending on the contamination source.

The pollutants mainly include metal ions and organic matters that are released from various sources such as medical, plumbing, agricultural, body care products, household chemicals, and industries. Among the toxic heavy metals that raise a serious concern are Cr^{2+}, Pb^{2+}, Hg^{2+}, Cd^{2+}, and others that are harmful to creatures.

To remove hazardous heavy metals' pollutants and enhance water quality, researchers used various adsorbent that are polymer based. Modifying existing polymers could be the simplest and most effective way to generate a low-cost adsorbent with high efficiency against metals and hazardous organic compounds.

Among all developed techniques, the adsorption removing approach has attracted the most attention. It has been particularly interesting to develop a superior adsorbent demonstrating a high adsorption capacity and low cost for removing various pollutants from contaminated waters. This study aims to develop cellulose with multi coordination site and zwitterionic functionality.

This study was planned to generate cellulose with multi coordination site and zwitterionic functionality. These criteria make it superior adsorbent for application in purification of polluted wastewater.

The target cellulose was designed to have coordination sites for toxic heavy metals and toxic anions such as nitrate. The method of making the polymer comprises three steps:

the first step involves adding an aldehyde functionality to cellulose powder by oxidation (Cell-Ald). In the second step Cell-Ald was crosslinked with a polyamine such 1,4-pheneylendiamine (PPD) to produce a 3D structure with multi coordination site, which then will be reacted with 1,4-butane sultone to form the target polymer cellulose with zwitterionic functionality (Cell-3D-ZWI). The polymer structure was confirmed by FT-IR.

The polymer was evaluated for their ability to adsorb Pb^{2+} ions. The percentage of metal adsorption was investigated as a function of Temperature, pH, adsorbent dosage, contact time, and initial concentration of metal ions. The high efficiency in adsorbing heavy metals from wastewater, with the maximum adsorption result for Pb^{2+} being 97.43% at pH ≈7.21, adsorbent dosage =20 mg, initial concertation of metal ion =10 ppm, contact time =20 min and temperature =20°C.

In addition, the adsorption isotherm, kinetics, and thermodynamics were measured. The thermodynamic parameters of Pb^{2+} adsorption is spontaneous ($\Delta G°<0$), exothermic process ($\Delta H°<0$) and the reaction occurs spontaneously at low temperatures ($\Delta S°<0$). All adsorption processes follow the pseudo- second order adsorption kinetics model (R^2= 0.99), which was established by the adsorption parameters, and these adsorptions were matched with the Freundlich isotherm of adsorption (R^2=0.89).

The target compound was prepared and identified by IR spectroscopy, it has good thermal stability, it adsorbed metals from wastewater at high efficiency.

Keywords: Cellulose, Water pollution, Wastewater treatment, Heavy metal, Lead, *p*-Phenylenediamine, 1,4-butane sultone, Zwitterions.

Chapter One
Introduction

1.1 General Review

One of life's most basic requirements is water. In the world, there are 0.3% of useable water resources [1]. Water is necessary for human survival and well-being and is significant to many economic sectors, also it is essential for sustainable ecosystem services. Water is one of the most convenient natural resources, because it is capable of recycling, storing, transporting and diverting [2].

However, due to human activity and economic growth, water resources are unevenly distributed in both geography and time, and they are under pressure and stress [3, 4]. There is significant water stress in many nations as a result of the negative effects of the global population growth, the implications of climate change, and changes in lifestyle [1].

In addition to severely reducing water supply per person, population growth and rising water demand would put pressure on biodiversity across the entire world environment. In addition to temperature, rainfall, evaporation rates, vegetation type, and water overflow are other significant elements that affect water availability. Additionally, there are currently significant challenges to fairly distributing the world's freshwater resources among and between nations [5].

A healthy environment, clean air, and pure water are becoming more and more rare [6]. Recent decades have seen a decline in water quality due to population growth, fast industrialization, and careless use of natural resources. Also among the major pollutants to be concerned about are organic matter, food, pharmaceuticals, personal care items, heavy metals, pigments, and plastics [7, 8].

Pollution occurs through the introduction of contaminants into the natural system. More than 200 million people on earth are harmed by toxic substances that are present as pollutants. 80% of diseases, as posted by the World Health Organization (WHO), are transmitted by water [9].

When harmful foreign elements enter the water stream, such as agricultural chemicals, pesticides, and fertilizers, or metals like lead or mercury, water pollution occurs [10]. In addition to reducing usage and drinking water, water pollution also destroys the lives of all aquatic life and reduces the biological diversity of the ocean, sea, lake, and aquatic ecosystems [1, 11].

Heavy metals have received the most attention from environmental scientists among all pollutants because of their hazardous nature. Natural water often contains minimal levels of heavy metals, but many of them are dangerous even at extremely low doses [12, 13].

Heavy metal contamination, such as that brought on by Lead (Pb), zinc (Zn), mercury (Hg), nickel (Ni), arsenic (As), copper (Cu), chromium (Cr), and cadmium (Cd) has recently received much interest because of their toxicity to human, environment and other creatures [14-16].

They are mostly produced in the medical, agricultural, plumbing, domestic, personal care, textile, tannery, and manufacturing industries [17, 18].

Heavy metals are hazardous due to their bioaccumulation, which is defined as an increase in chemical concentrations in a biological organism over time relative to environmental chemical concentrations. As previously indicated, heavy metal ions are not biodegradable. They can influence a variety of organisms directly or indirectly due to biomagnification, and they are stable. They can cause a serious health problems including nervous system diseases, cancer, organs damage (lungs, kidneys, liver, esophagus, stomach) and skin, even when they are only present in minute amounts [19-23].

The threshold limit value (TLVs) of toxicity, which is known as the average concentration toxic substance concertation in air in which a normal person may be exposed to for 8 h/week for their life time without feeling any negative effects, is related to the inhalation toxicity [24].

When the concentration of a heavy metal in water surpasses a certain level, it is considered a pollutant and harms living organisms. Based on its toxicity, each hazardous metal has a threshold limit value [13, 25].

Chronic exposure to hazardous metals has negative effects that become noticeable after a period. Cadmium causes cerebrovascular infarction, cardiac failure cancers, lung cancer, osteoporosis and emphysema [26, 27].

Copper can cause capillary damage, renal damage, hepatic, irritation and depression, of the central nervous system are all carried on by copper [28, 29]. Mercury damages the nervous system, the kidneys, and induces mutagenesis [30].

Zinc has been associated to prostate cancer, kidney failure, icterus, anemia and liver failure [31]. Also, Anemia, anorexia, vomiting, liver and lung damage, loss of appetite, damage to the digestive and urinary systems, harm to the developing fetal brain, and degradation of the nervous and circulatory systems can all result from lead poisoning [32, 33].

As a result, it became important to remove toxic metals from water because they disturb human organelles and are non-biodegradable pollutants that are consumed through the food chain [34].

1.2 Wastewater purification and reuse

It is essential to have access to clean drinking water since contamination not only reduces the amount of freshwater that can be used, but also has an effect on both human health and the ecosystem [35].

The most crucial component for survival is water, which is composed of two hydrogen atoms connected by an oxygen atom. A variety of contaminants, including dangerous compounds used in human activities, naturally occurring minerals and chemicals, and contaminants that alter flavor, smell, and color, among others, could pollute it. In order for water to be appropriate for its intended application, contaminants must be removed or reduced through treatment. Making water suitable and acceptable is the process of water treatment [36].

The ability to treat and reuse water provides advantages that serve as the primary motivations for developing reuse programs. These advantages include increased agricultural production, less energy use for water production, treatment, and

distribution, and major environmental advantages like decreased nutrient loads to receiving waters due to the reuse of treated wastewater [37].

As a result, water purification has become a global crisis that must be resolved in order to maintain ecological stability and improve public health. To solve this issue, finding effective water treatment systems that are high-performing, affordable, and energy-efficient is very important. The literature reports a number of methods for removing harmful heavy metals from wastewater.

The most efficient of these are adsorption and precipitation [38]. The most consideration was given to the adsorption method because it is both highly efficient and inexpensive [39].

For commercial application, ideal adsorbents should have the following characteristics; Large adsorption capacity, high adsorption rate, cost-effectiveness, environmental safety, easy of separation, robustness, and reusability [40].

One of the most studied adsorbents for the removal of metals from wastewater is activated carbon; nevertheless, the high costs associated with material processing have made it less desirable in some situations [41].

Naturally produced materials like clay [42], zeolites [43], and peats [44], were also investigated as toxic metal adsorbents. industrial residue that includes fly ash, sludge, red mud, and metal hydroxide [45].

As a consequence, it has been proposed that inexpensive, environmentally friendly adsorbents made from agricultural waste would make good alternatives for treating wastewater [46, 47].

Among the natural based adsorbents that received the highest attention are cellulose, lignin, chitosan and hemicellulose. Cellulosic based adsorbents specially those obtained from waste form Kenaf waste [48], cotton [49], wheat [50], sawdust of wood [51], husk form rice [52] were already evaluated as adsorbents of various metal ions such as Cd^{2+}, Co^{2+}, Cu^{2+}, Mg^{2+}, Sr^{2+}, Al^{3+}, Ni^{2+}, Mn^{2+}, Cr^{3+}, $Zn^{2+}$and Pb^{2+} ions.

However, they may be produced significantly more cheaply than activated carbon, despite having a lower adsorption capacity due to its larger surface area. They are particularly effective at removing heavy metal ions from wastewater while being ecologically friendly and economically feasible [53]. In recent years, a breakthrough was made in polymeric nanotechnology for generating promising nanomaterials as an adsorbent for toxic metals. Among these is cellulose nanocrystals (CNCs), which is unique regarding functionality, high surface and rigidity, which resulted in improved purification efficiency. Despite the significant development in nanocellulose adsorbents, several nanocellulose derivatives have still not been investigated as metal adsorbents [54].

1.2.1 Polyzwitterions

Recently, several innovative ideas have been published in the literature for the instantaneous removal of heavy metal ions from polluted water using cellulose with zwitterionic functionality as the adsorbent [55-60].

Zwitterions have both positively and negatively charged group as a pendent-side groups. Polyzwitterions material bear on their repeat units equal number of anionic and cationic groups [61]. This type of material represents a special type of polyampholytes presenting a very specific properties [62-65]. In these types of materials, the ionic groups are efficient over a wide range of pH values.

So, both charges positive and negative are present on the repeat unit, the total charge of polyzwitterions is zero, yet there is no association between them **Figure1.1** [62-66]. They are used as ionomers in food waring applications [67-70], in fibers due to strong interactions they form with the dye stuffs [71-73]. Due to their high tolerance to saline environments, they are used as a rheology modifier [74, 75].

Figure 1.1

model of a polyampholyte (left) and polyzwitterions on the (right)

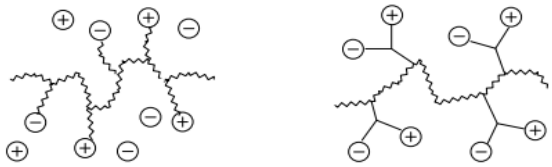

Note. The image was created to represent model of a polyampholyte and polyzwitterions. “by Biehl, P., et al., Synthesis, characterization, and applications of magnetic nanoparticles featuring polyzwitterionic coatings. 2018. 10(1): p. 91.” [76].

Examples on natural zwitterionic compounds are shown in **Figure 1.2** From left to right: phospholipid 1,2-dimyristoyl-sn-glycero-3-phosphatidylcholine (DMPC), trigonelline, ectoine, betaine, 3-dimethylsulfoniopropionate (DMSP), arsenobetaine [77-79].

Figure 1.2

Examples on natural zwitterionic compounds

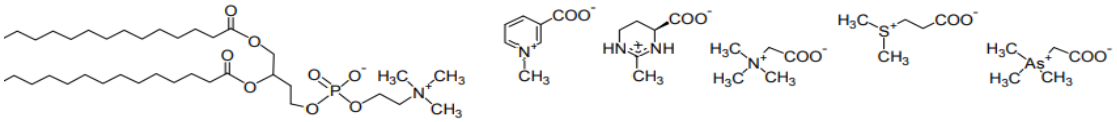

Note. The image was created to represent natural zwitterionic compounds. “by Laschewsky, A.J.P., *Structures and synthesis of zwitterionic polymers.* 2014. **6**(5): p. 1544-1601.” [71]

The presence of such functionality structure allows the adsorption and recovery of heavy metal ions from wastewater by the electrostatic effect [80-82]. The main cause for the lack of a wider use of this methodology is the complexity of synthesizing a cellulose-based adsorbent with a high degree of substitution of with zwitterionic functionality. Therefore, it is necessary to design and synthesize a cellulose-based adsorbent with a high degree of substitution of amino and sulfonate groups in order to create adsorbent with high efficiency for anionic and cationic heavy metals.

Therefore, this research, offers a cellulose-based adsorbent with high degree of pendant groups composed of ammonium, amine and sulfonate, presence of these groups on same repeat unit create coordination sites for metal and zwitterion functionality.

The target cellulose based-zwitterionic will be synthesis by oxidation then crosslinking of cellulose then reacting with 1,4-butane sultone. This target polymer will be evaluated as an adsorbent for Pb^{2+} under various adsorption conditions. The mechanism of adsorption of adsorbents for the metal removal of the target ions from an aqueous medium will be also studied.

1.2.2 Adsorption technique

Heavy metal pollution of water is a serious issue because of the harmful effects that heavy metals have on the environment and on living creatures, particularly because of their tendency to bioaccumulate and persistence in nature. Adsorption technologies are one technique that has been developed recently to purify natural water from heavy metals and industrial waste. Conventional adsorbents, such activated carbon, sometimes produce hazardous sludge that needs to be post-treated while also being less effective. Although nanotechnology adsorbents have recently been employed in water purification, their practical applications in the removal of hazardous heavy metals are limited because of the complicated synthesis procedure and high cost [83].

A suitable adsorbent for the removal of heavy metals should have a low cost, stability, ease of separation, simplicity of design, high absorptivity, high adsorption capacity, and good reusability [84, 85].

Adsorptions take place when an adsorbate leaves the liquid phase of the contaminated mixture and bond to the adsorbent surface through a physical or chemical interaction. According to adsorption science, the material that is adsorbed on the solid surface is known as an adsorbate, while the solid surface is known as adsorbent. Adsorbate can be dissolved solids, a gas, or a liquid. While adsorbent can be either a liquid or a solid [86].

Adsorption technique efficiency is influenced by several variables. These factors include the adsorbent's surface area, activation energy, as well as the type of adsorbent and adsorbate. It also depends on the conditions of the experiment. such temperature, pressure, and pH level [87].

New intermolecular forces of attraction are created between the adsorbent and the adsorbate as a result of this purification process. Two categories of adsorption can be distinguished based on the nature of these forces.

1. **Physical Adsorption (Physisorption)**

   This kind of adsorption has a wide range of features. These are dipolar interactions, which are weak intermolecular forces of bonding. Physical type of adsorption also requires very little activation energy because it has a lower heat of adsorption. Since it is not highly selective, physisorption creates multi-molecular layers [88].

   Additionally, this type of adsorption is reversible since the adsorbate molecule is free to roam around the adsorbent surface instead of being fixed in one place. This allows for the possibility of adsorbate recovery [88].

   Physisorption frequently takes place with no heat and is readily reversible by raising the temperature or lowering the pressure [89].

2. **Chemical Adsorption (Chemisorption)**

   The following are some of chemisorption's characteristics: Chemical bonds, like covalent and ionic bonds, are strong forces of interaction. Additionally, it has a relatively high adsorption enthalpy, which means that this adsorption typically needs a high activation energy to occur [90]. Furthermore, chemisorption is irreversible, specific, and occurs at high temperatures [91].

1.2.3 Heavy and Toxic Metals

Metals that are "bad" for the environment are referred to as "heavy transition metals." Based on the atomic weight, atomic number, density, or other characteristics of the elements or their compounds, it might indicate a variety of things [92].

Metals with an atomic number (Z) more than 20 and an elemental density greater than 5.0 g/cm^3 are classified as heavy metals. The 51 elements of the periodic table are categorized by scientists as heavy metals based on this classification. Three groups of heavy metals are distinguished: radionuclides, precious metals, and toxic metals [93, 94].

Heavy metals, in contrast to organic-based contaminants, cannot be biodegraded once they are released into the environment. For the rest of their lives, they will keep harming the environment, water, and air. Reduced metal toxicity, mobility, and bioavailability are the fundamental methods for reducing pollution. While some trace amounts of

transition heavy metals are necessary, the vast majority are toxic to all living things [95].

Five main factors contribute to the presence of heavy metals in aquatic systems: geological weathering, industrial processing, utilization of metals compounds and metal`, combustion of fossil fuels, and metal leaching from rubbish and solid trash dumps. Lead, cadmium, mercury, and arsenic are the heavy metals that have the greatest negative effects on human health. International institutions like the World Health Organization regularly monitor the effects of these metals on human health as a result of extensive research on them. Humanity has been using heavy metals for a very long time. Heavy metal exposure is still present and even increasing in some parts of the world, primarily in developing nations, despite the fact that heavy metal pollution has declined over the past 100 years in the majority of developed nations [96].

In general, a variety of factors affect the toxicity of heavy metals. These include age, speciation, total dose absorbed, and exposure route. Large doses of any heavy metal may result in either chronic toxicity with a long-term effect or acute toxicity with a short-term effect. Some heavy metals may be hazardous in higher concentrations even though they are innocuous or even vital for life at trace amounts. This is true, for example, with copper and zinc, which necessary in trace amounts for living things, have poisonous consequences when present in higher concentrations. The toxicity of a heavy metal is inversely associated with its TLV, meaning that metals with lower TLVs will be more poisonous than those with higher TLVs [97, 98].

1.2.3.1 Lead

A naturally occurring element, has a density that is higher than the bulk of other materials. Freshly cut lead has a silvery appearance with a trace of blue, but when it is exposed to air, it oxidizes and turns dark gray. Among all stable elements, lead has the highest atomic number. It is not very reactive, and when its oxides come into contact with acids and bases, they form covalent bonds [99].

Typically, lead compounds are found in the +2 oxidation state , rather than the +4 oxidation state that is common for lighter carbon group members. It was used in many different industries, including electroplating, metallurgy, chemicals, and many more.

Hazardous heavy metal lead can harm your bones, brain, blood, kidneys, thyroid glands, and other organs. The discharge's toxic nature and presence of lead have additional negative effects, also at extremely low levels. Lead metal levels in water might be dangerous [99].

Pb^{2+} released into the environment eventually is transported to human organs through the food chain or drinking water. As a result, there may be danger to the neurological, hematologic, and reproductive systems of humans [100].

Lead is a toxic chemical that accumulates in bones and soft tissues, harming the neurological system. Even if blood levels are quickly restored with treatment, neurological disorders like brain damage can still happen [99].

Finally, there are other lead sources that can result in lead poisoning, including lead paint, lead-contaminated household dust, soil, water, and food. All sources of lead should be controlled or eliminated because lead accumulates in the body [100].

1.3 Cellulose

The most abundant and renewable biopolymer on earth is cellulose. The formula for this organic polymer is $(C_6H_{10}O_5)_n$. The homopolysaccharide molecular structure of cellulose is a linear polymeric chain of thousands of the monomer D-anhydroglucopyranose joined by – a glycosidic linkages. The chair shape of the six-membered heterocyclic -D-anhydroglucopyranose is the most common form [101].

Figure 1.3

Molecular structure of cellulose polymer

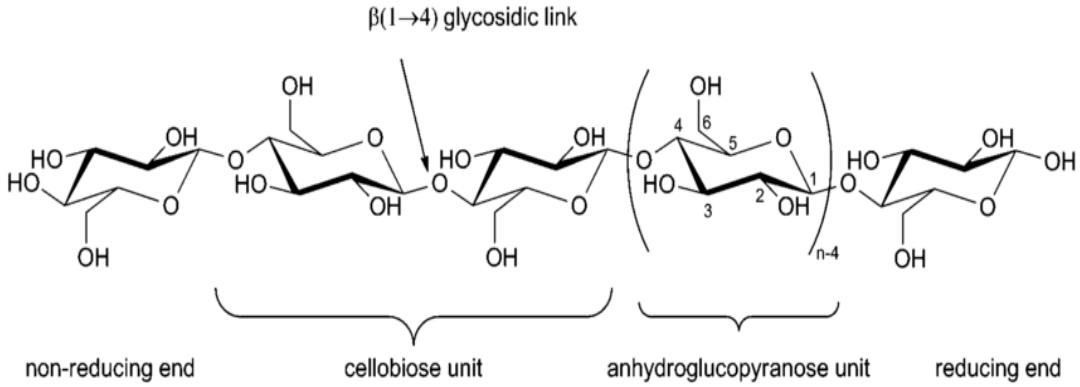

Note. The image was created to represent molecular structure of cellulose polymer. "by Eyley, S. and W.J.N. Thielemans, Surface modification of cellulose nanocrystals. 2014. 6(14): p. 7764-7779." [102].

The many hydroxyl groups found in cellulose can be broken down into three groups: the primary hydroxyl group is C-6, while the secondary hydroxyl groups are C-2 and C-3 [103].

These numerous hydroxyl groups form hydrogen bonds with oxygen atoms near or inside the same backbone (intra molecule hydrogen bonding), causing the chain to come into touch with one another and producing microfibrils with a high tensile strength. Heavy metal ions have an affinity for hydroxyl groups [103].

Figure 1.4

Molecular structure of cellulose polymer showing H-Bonding

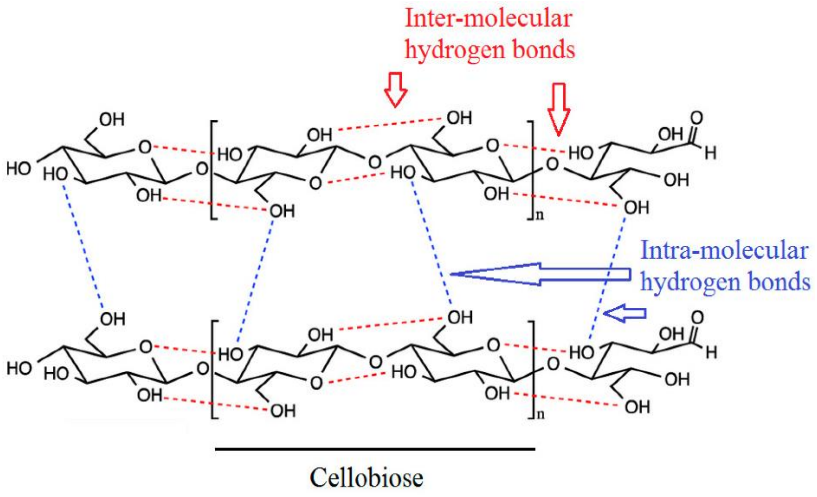

Note. The image was created to represent H-Bonding in molecular structure of cellulose polymer. "by Baghaei, B. and M.J.M. Skrifvars, All-cellulose composites: A review of recent studies on structure, properties and applications. 2020. 25(12): p. 2836." [104]

Cellulose has a molar mass of 162.1406 g/mol per glucose unit, a density of 1.5 g/cm^3, a melting point of 260–270 ℃, is biodegradable, and has hydrophilic regions that make it insoluble in water and most organic solvents [105]. In nature, cellulose is present in a wide range of creatures, including plants, bacteria, fungi, invertebrates, amoebas, minerals, and many marine organisms.

However, the primary source of cellulose is plant fiber. Most organisms have cellulose as a structural element of their cell walls. To form porous biofilms, certain bacteria also excrete bacterial cellulose. 1011–1012 tons of relatively pure cellulose are manufactured each year. Cellulose makes up 90.0% of cotton, and a dried hump contains roughly 57.0% of it [106].

The number of repeat units (DP), which denotes the number of repeating monomers, is represented by the number n in the chemical formula for cellulose $(C_6H_{10}O_5)_n$. The degree of polymerization affects a number of cellulose properties (chain length). In plant cells, cellulose has a DP of roughly 15000 units and about 10,000 units in wood. Mechanical strength and melting temperature rise as DP rises [107].

There are crystalline and amorphous areas in cellulose fibrils. The cellulose crystalline structure has an impact on cellulose properties. For instance, As the proportion of

crystalline rises, the cellulose's strong and tightly packed hydrogen bonding network causes the amorphous fraction to become less flexible. Numerous cellulose amorphous result from the wide orientation of the hydrogen bonding networks [108].

Flexible cellulose nanofibrils are produced through enzymatic or chemical oxidation of cellulose fibrils. Short rigid cellulose nanocrystals will be produced if amorphous regions hydrolyze with a strong acid (few nm in length). This substance possesses a lot of useful qualities [108].

Since it is readily available, nontoxic, chemically, and thermally stable, biodegradable, and has a high tensile and compressive strength, cellulose is an excellent choice for adsorbing metals. The linear, long chain of cellulose polymer is filled with many hydroxyl groups that extend from the chain and produce intermolecular hydrogen bonds, which improve the interaction of neighboring cellulose molecules. If the hydroxyl groups are changed, many derivatives of cellulose can be produced and employed in an infinite number of applications [109].

1.3.1 Chemically modification of cellulose for heavy metals removal

When cellulose is chemically modified, the hydrogen bonds are broken, the crystal structure is reduced, and more efficient binding sites (OH groups that are more attackable by other functional groups and enhance adsorption) are generated [103].

The two main techniques for cellulose modification are:

1) The formation of a cross-linking network (gel) through chemical bonding of the OH and NH_2 groups, which is insoluble in water.
2) Creating hybrid materials by using grafting reaction to control polysaccharide movement on a surface [110].

Various cellulose polymers that have been chemically modified were developed and used in the purification of water. Cellulose was obtained from the solid part waste produced by the olive industry to produce the polymers (NCC-PBG-A and NCC-PBG-B) **Scheme 1.1** [108]**.**

The first polymer NCC-PBG-A, which contains both groups amine and imine, was produced by first oxidizing the isolated cellulose and then reacting it with

phenylbiguanide. Then, a borohydride (BH_4) was used to reduce the imine groups to produce a new polymer NCC-PBG-B that was loaded with amine functionality. The polymers were examined for their ability to remove Cu^{2+} and Pb^{2+} ions from sewage. With regard to these ions, both polymers showed higher adsorption effectiveness [111].

Scheme 1.1

(a)structure of modified cellulose NCC-PBG-A,(b) structure of modified cellulose NCC-PBG-B

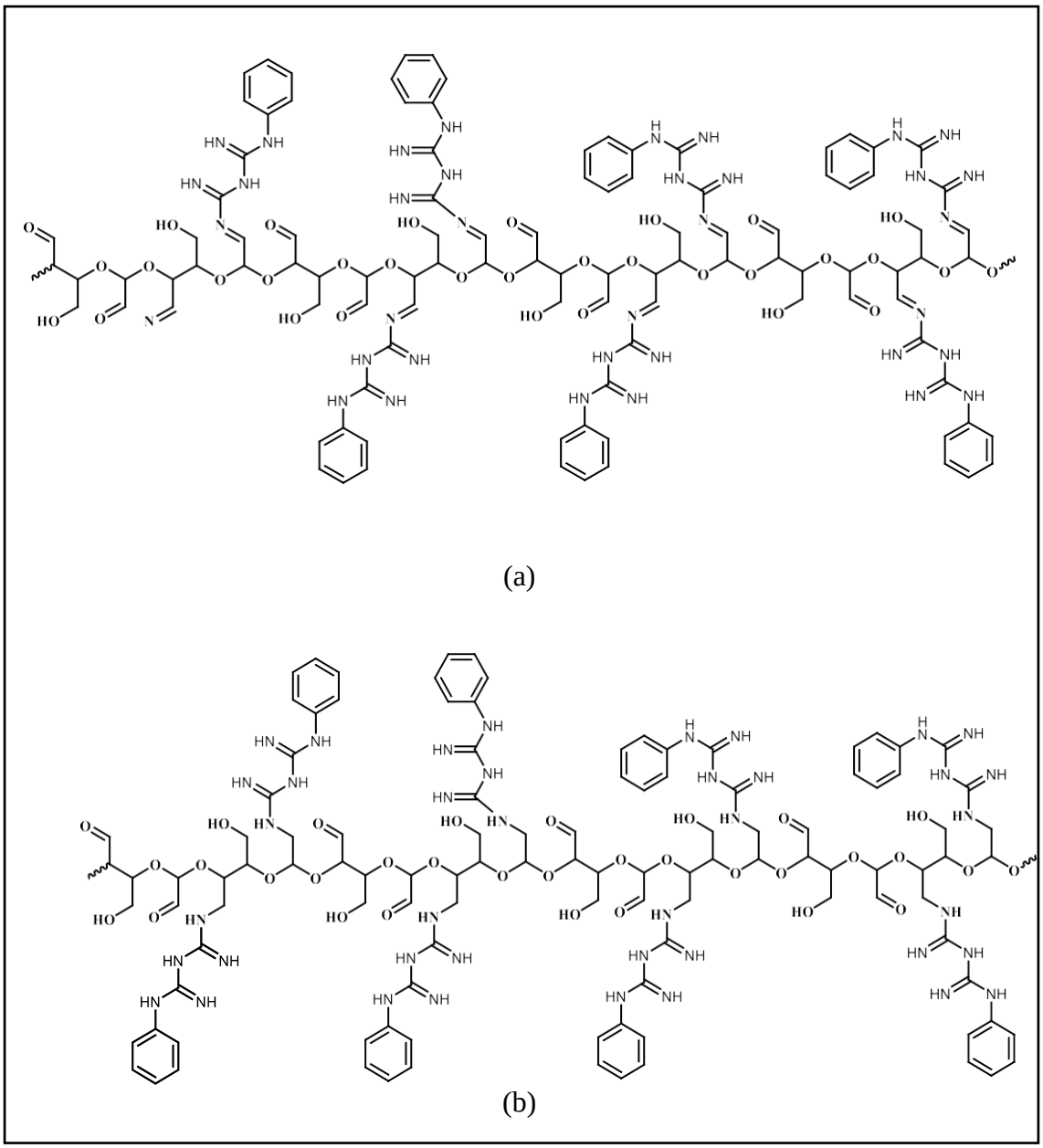

(a)

(b)

Note. The image was created to represent structure of modified cellulose NCC-PBG-A and NCC-PBG-B. "by Peng, B.L., et al., Chemistry and applications of nanocrystalline cellulose and its derivatives: a nanotechnology perspective. 2011. 89(5): p. 1191-1206." [108].

Researchers developed, manufactured, and evaluated multidentate chelating cellulose polymers with excellent efficacy for toxic metal ions in water. The synthesis involved reacting microcrystalline cellulose (Cell-AA), which was taken from the solid waste of the olive industry, with tert-Butyl acetoacetate.

This formed cellulose with β-ketoester functionality, which was then reacted with aniline and the amino acid glycine to produce Cell-AN and Cell-GL, respectively.The Cell-AA and Cell-GL polymers had the highest Pb^{2+} efficiency at concentrations of 10.0 ppm, 50.0 mg at 9.0 pH and at 30 °C after being shaken for 120 minutes. At almost the same prior conditions, the Cell-AN polymer showed the best efficiency toward Pb^{2+} at 86.7% **Scheme 1.2** [112].

Scheme 1.2

(a) structure of Cell-AA, (b) Cell-AN, (c) Cell-GL

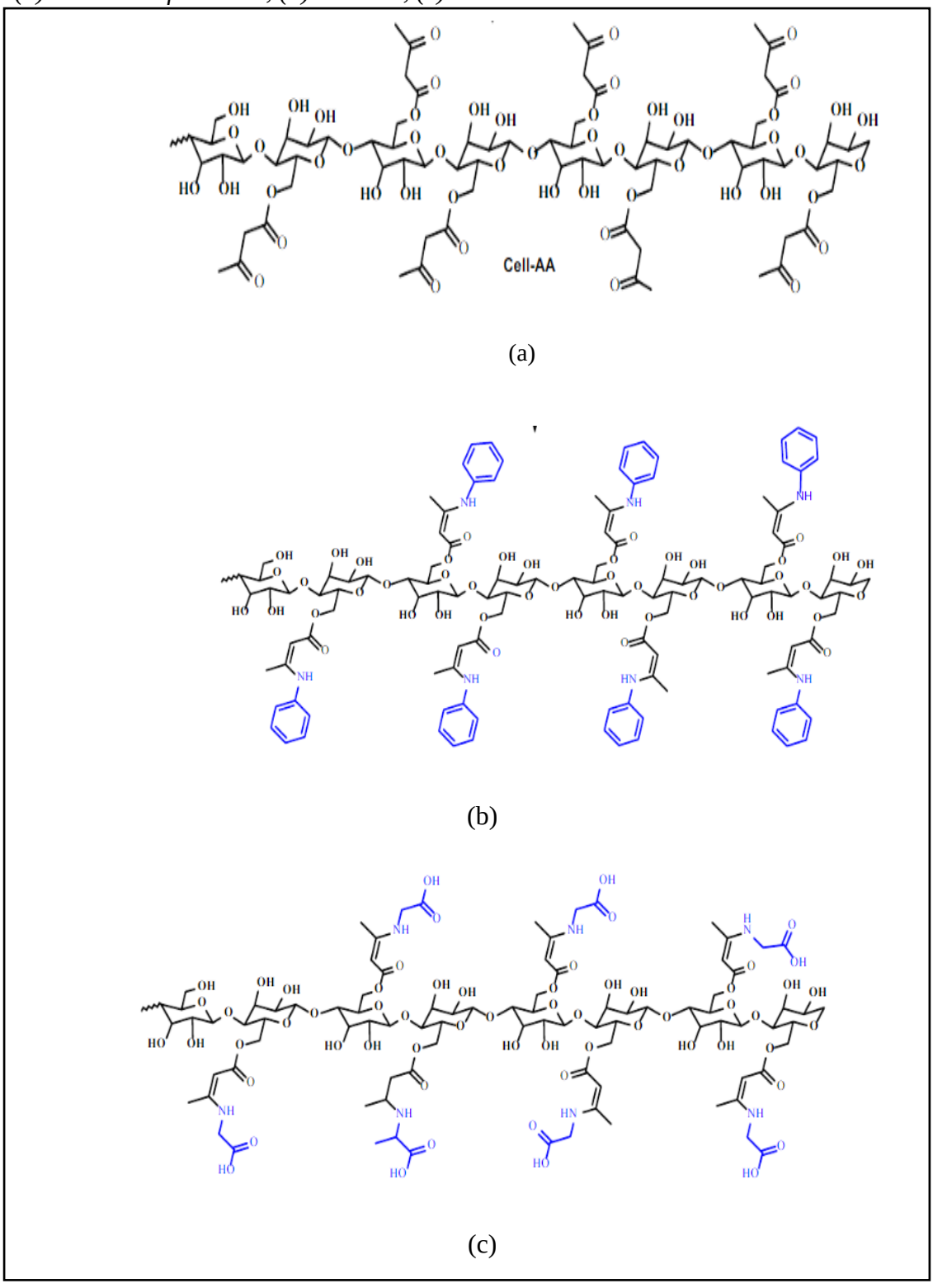

Note. The image was created to represent structure of Cell-AA, Cell-AN and Cell-GL. “by Nairat, N., et al., Cellulose polymers with β-amino ester pendant group: design, synthesis, molecular docking and application in adsorption of toxic metals from wastewater. 2022. 16(1): p. 1-21.” [112]

Cellulose was used as one of the main ingredients in a three dimensional crosslinked polymer that was used to remove dangerous metals from water. Carboxymethyl cellulose (CMC) was first made by combining cellulose with chloroacetate and a solution of sodium hydroxide in isopropyl alcohol.

At approximately 160 °C, β-cyclodextrin and the generated CMC were crosslinked. Three crosslinked cellulose and cyclodextrin polymers (co-β- CMC- CD) A, B, and C were synthesized and manufactured. When synthesizing the polymers, various ratios of the materials were used [113].

The ability of the three polymers to remove Pb^{2+} from a water solution was investigated. At pH 7.5, 20°C, and 0.05 mg/L concentration, the maximum adsorption efficiency was achieved. Compared to the other two polymers, Polymer B had a lower efficiency toward Pb^{2+}.

The outcomes also indicate that Pb^{2+} adsorption takes place on the surfaces of polymer A in a pseudo-second-order model. The adsorption process $\Delta G°$ value was negative, according to thermodynamic experiments, suggesting a spontaneous adsorption process [113].

Scheme 1.3

Structure of co-β-CMC-CD

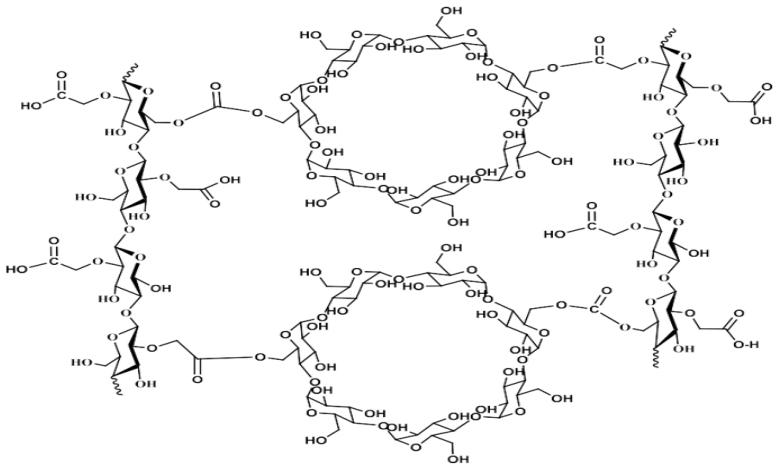

Note. The image was created to represent structure of co-β-CMC-CD. "by غ ،شقدان. and ابتهال, Anionic Microcrystalline Cellulose For Removal of Pb+ 2 From Waste Water Purification. 2020, جامعة النجاح الوطنية." [113].

Novel adsorbent based on cellulose was created by functionalization of Nanocrystalline Cellulose (NCC) to make it a potential novel metal ion adsorbent. The cellulose used in this study derived from olive industry solid waste (OISW), which was hydrolyzed into nanocrystalline form, then oxidized to cellulose dialdehyde (CDA), which was then reacted with 1,4-phenyldiamine under mild conditions to produce the final cellulose diamine (cell-p-PDA) product **Scheme 1.4** [114].

The produced cell-p-PDA was examined as an adsorbent of the metal ions $Pb^{2+}$and Cu^{2+} from wastewater, and at a pH value of 8.3 and at room temperature, it displayed excellent eficiency toward both metals. Additionally, an actual sample of sewage containing more than 20 elements was successfully processed by Cell-p-PDA. The different functionalities on the polymer surface and the potential semi-crown ether structure produced by cross-linking the cellulose chain with 1,4-phenylene diamine may be responsible for the excellent extraction efficiency of the cell-p-PDA polymer. According to the kinetic analysis, the metal ion adsorption by cell-p-PDA was pseudo-second order and followed the Langmuir isotherm model [114].

Scheme 1.4

Structure of cell-p-PDA polymer

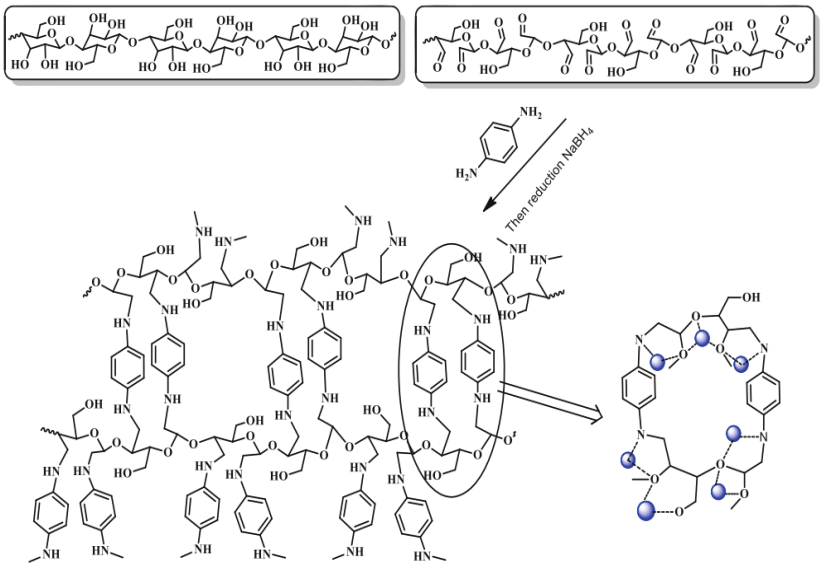

Note. The image was created to represent structure of cell-p-PDA polymer. “by Hamed, O., et al., Synthesis of a cross-linked cellulose-based amine polymer and its application in wastewater purification. 2019. 26: p. 28080-28091.” [114].

A new cellulose amine polymer was synthesized using a three-step technique using cellulose and o-phenylenediamine as a chelating agent. In this procedure, cellulose is first converted using aldehyde, then to imine, and that was reduced to amine by sodium borohydride.

As seen in **Scheme 1.5**, this cellulose derivative has several coordination sites. In a sewage sample, the cellulose polymer with the amine moiety served as a new adsorbent for toxic metal ions like Fe^{3+}, $Pb^{2+}$and others[115]

The high efficiency was associated with the presance of many functional groups such as hydroxyl, ether, aromatic, and amine. The effectiveness of the cellulose amine polymer's adsorption on Fe^{3+} and Pb^{2+} was examined. According to kinetic studies, the adsorption isotherm corresponds to the Langmuir isotherm model [115].

Scheme 1.5

Structure of cellulose amine polymer

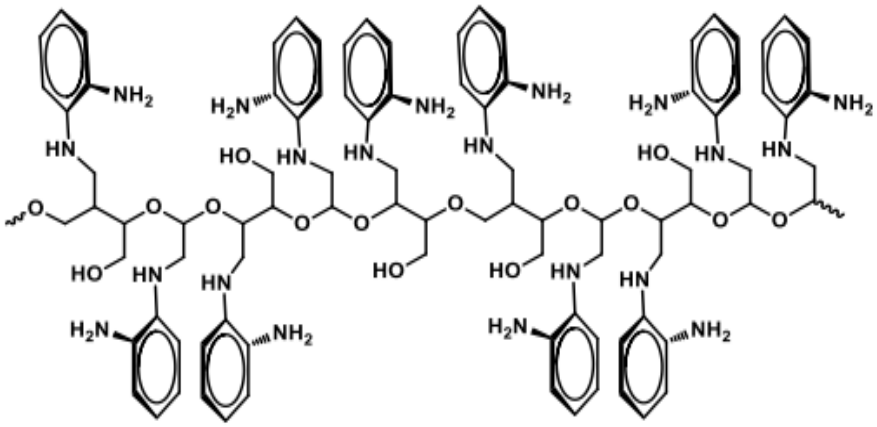

Note. The image was created to represent structure of cellulose amine polymer. “by Deghles, A., et al., Cellulose with bidentate chelating functionality: an adsorbent for metal ions from wastewater. 2019. 14(3): p. 6247-6266.” [115]

First, cellulose with dialdehyde groups was generated from cellulose that had been extracted from the solid waste of the olive oil industry by oxidation with sodium periodate, followed by a reaction with p-diaminobenzene to create cellulose imine, which was subsequently hydrognetaed to cellulose diamine by a reaction with sodium borohydride. Prepared cellulose diamine has a distinctive molecular structure; the diamine molecule binds the cellulose chains to generate a type of crown amine [116].

The nitrogen and oxygen binding sites in the crown amine cages are distributed around the ring. These locations show a particularly strong metal affinity. Toxic elements from wastewater were removed using the produced cellulose diamine. The optimal conditions were a temperature of 30 ℃, a time about 120.0 min, a pH about 4, and a dosage of 0.50 g. The results generated by kinetic study demonstrated that the rate of adsorption follows a pseudo-second-order [116].

In another study, cellulose powder was utilized to produce magnetic cellulose nanocrystalline (MNCs), which had been used as selective magnetic adsorbents to remove methylene blue from water. In this study, OISW was utilized to make the cellulose powder [46].

By using acid hydrolysis, the extracted cellulose was converted into NCs. NCs were treated with a solution of $FeSO_4$, $FeCl_3.6H_2O$, and H_2O in order to produce MNCs using the colloidal suspension method. For inorganic nanoparticles from aqueous solutions, MNCs act as an efficient, economical, and rapid adsorbent. According to thermodynamic analyses, the adsorption process occurs spontaneously at different temperatures [46].

1.3.2 Cellulose as a metal adsorbent

Because of increased urbanization, population expansion, and economic development, there is an increase in the amount of produced wastewater and its overall pollutant load globally. Our primary objective in developing this work was to create a novel practical method of extracting heavy metals using cellulose-based materials as adsorbents. Wastewater needs to be cleaned up, with a heavy metal elimination goal in mind [117].

There are a number of widely used techniques for heavy metal removal from water, but these techniques have some limitations. The most simple, sustainable, and effective technology for wastewater purification was adsorption. As a result, efforts were directed on using inexpensive adsorbents. Due to its crystallinity and hydrogen bonding, cellulose is a natural, recyclable, biodegradable, non-meltable, and insoluble in most solvents. Cellulose is a good metal adsorbent that is easily chemically modified. because cellulose has a lower adsorption capacity for heavy metals [118, 119].

1.4 p-Phenylenediamine

p-Phenylenediamine is an organic compound with The molecular formula is $C_6H_4(NH_2)_2$ while the molar mass is 108.1 g /mol [120]. This aniline derivative is a white solid, however samples may turn darker as a result of oxidation in the air. In engineering polymers and composites like kevlar, it is mostly used as a constituent. It is also a component of hair dyes, and it is sometimes used in henna [121].

Poly phenylenediamine , a less expensive diamine derivative of polyaniline (PANI), has also attracted attention and that was related to its high oxidative polymerization and large number of imine and amine groups. A lot of interest has been given to poly phenylenediamines because they contain both cationic and redox characteristics [122].

Due to their numerous applications, high electroactivities, and high thermal stability, aromatic amine polymers have recently been receiving a lot of attention. As a result of oxidation reduction reactions and chelations property of the amino and imino groups, PPDs have demonstrated a strong affinity for metal ions. PPD with plenty of amine groups can reduce the valence states of absorbing metallic pollutants by acting as electron donors [122]. The structural formula of PPD is shown in **Figure 1.5**.

Figure 1.5

Chemical structure of P-Phenylenediamine

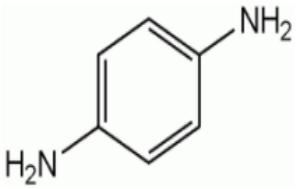

Note. The image was created to represent chemical structure of P-Phenylenediamine. “by Chong, H., et al., Para-phenylenediamine containing hair dye: An overview of mutagenicity, carcinogenicity and toxicity. 2016. 6(5): p. 1000403.” [123].

1.5 Scope of This Study

The general aims of this research is to synthesize zwitterionic cellulose with multi coordination site and use it for extracting toxic ions (cationic and anionic) present in wastewater and other contaminated water.

The sub aims include:

1. Develop a chemical method to produce 3D cellulose with multi coordination sites
2. Develop a chemical method to add the zwitterionic functionality to the 3D cellulose.
3. Evaluate the efficiency of prepared polymer as an adsorbent for toxic cationic metals and nonmetal anions.

4. Use different spectroscopic methods to describe the new adsorbent.

Chapter Two
Experimental Part

2.1 Materials

Chemicals and reagents used in this work were purchased from Sigma-Aldrich chemical company (Jerusalem) and used as received. The chemicals include Sodium periodate ($NaIO_4$), Methanol, 2-Propanol, Hydroxylamine hydrochloride ($NH_2OH.HCl$), p-Phenylenediamine, Acetic acid, Sodium borohydride ($NaBH_4$), 1,3-Propane sultone.

All reagents used were of analytical grade. Deionized water was used to prepare all solutions. Cellulose used in this work was extracted from olive industry solid waste (Jeft) by a chemical process that was developed at the laboratories of An-Najah National University-Nablus/Palestine.

2.2 Instruments

The following equipment were used in this research: pH meter (JENWAY, model: 3510), water shaking bath (Daihan Labtech, 20.0 to 250.0 rpm Digital Speed Control), Fourier-Transform Infrared Spectrophotometer (FT-IR) (Nicolet iS5, iD3 ATR, Thermo Fisher Scientific), Flame Atomic Absorption Spectrometer (ICE 3000 series AA System, Thermo Scientific), and Inductively Coupled Plasma Mass Spectrometer ICP-MS (ICE 3xxx C113500021 v1.30).

2.3 Polymer synthesis

2.3.1 Activation of microcrystalline powder cellulose

The first step in the process involves activation of cellulose. This activation was achieved by adding 10.0 g microcrystalline cellulose to 500 ml distilled water and kept stirring by a magnetic stirrer for 6 hour.

2.3.2 Oxidation of microcrystalline cellulose

This step involves oxidation of cellulose to cellulose-2,3-diladehyde (Cel-Ald). Activated microcrystalline powder cellulose (10.0 g, 0.062 mol of anhydroglucose repeat unit) and an excess of $NaIO_4$ (16.0 g, 0.075 mol) was added to a 500.0 mL of distilled water in a beaker (1000 ml). The beaker wrapped completely with aluminum foil.

After being stirred by a mechanical mixer in a hot water bath (40.0°C) for 24.0 hours, the beaker was then filtered, and any side products or remaining chemicals were removed by repeatedly washing the product in water and methanol.

The product was analyzed by FT-IR after dried at room temperature.

2.3.2.1 Degree of substitution

To 50.0 ml of propan-2-ol, The oxidized cellulose was put in 1.0 g. 10 minutes of stirring the suspension were followed by the addition of 10 mL of distilled water. Using a 5.0% diluted solution of HCl, the pH of the mixture was decreased to about 3.5, and it was then stirred for an additional 30.0 minutes.

Hydroxylamine hydrochloride was prepared as an aqueous solution ($NH_2OH.HCl$, 5.0% by mass). Using an HCl solution that was 5.0% diluted, the pH was changed to 3.5.

The two liquids mentioned above were combined and stirred for 12 hours. Then, 0.5 N NaOH was added to the solution to titrate it to pH 3.5 [111, 124].

The aldehyde content was determined by applying the following equation:

$$[Ald] = \frac{(V_{NaOH} \times N_{NaOH} \times 162)}{W_{OC}} \qquad \textbf{Eq. 1}$$

Where;

[Ald]: degree of substitution (mmol/AGU).

V_{NaOH} : volume of NaOH (mL).

N_{NaOH} : normality of the NaOH (eq/L).

W_{OC} : oxidized cellulose dry weight (g).

2.3.3 Crosslinking of cellulose 2,3-dialdehyde

The polymer that carries imine and amine functional groups was produced by reacting cellulose dialdehyde with PPD to form modified cellulose.

2.3.3.1 Preparation of 2,3-cellulose diimine

Oxidized cellulose powder (1.0 g, 0.0062 mol) and excess PPD (1.0 g, 0.0062 mol) were added to a 100.0 mL round bottom flask with a magnet stir bar, 50.0 mL of methanol was added as the solvent. Then to it was added a 1.0 ml of acetic acid as a catalyst. A condensation reaction occurs at about 70 ℃ for 24 hr. After reaction was completed, the imine product was filtered and repeatedly methanol washed, was then examined by FT-IR after drying at room temperature.

2.3.3.2 Reduction of 2,3-cellulose diimine to 2,3-cellulose diamine

Imine conversion to an amine was carried out using sodium borohydride (0.5 g, 0.15 mol) that was added to a suspension of cellulose diimine (2.0 g, 0.029 mol/AGU) in 50.0 mL of methanol in 100 ml round bottom flask fitted with a magnet stir bar. The reaction mixture was stirred at room temperature for 1 hr then refluxed for 24 hr. After that the reaction was cooled using ice water bath and during that was treated with 2.0 ml water dropwise, then stirred for 30 min. The generated precipitate was suction filtered, repeatedly rinsed with methanol, and allowed to dry at room temperature and the crosslinked cellulose (Cell-X) was analyzed by FT-IR.

2.3.4 Preparation of cellulose with zwitterionic functionality

Cellulose diamine was added to a round-bottom flask (100 ml) equipped with a magnet stir bar (1.0 g, 0.0037 mol).1,3-propane sultone (0.45 g, 0.0037 mol) and 50 ml THF was added to the flask. For 24 hours, the reaction mixture was refluxed.

Then the target cellulose with zwitterionic functionality (Cell-X-ZWC) was filtered, washed with THF, dried at room temperature before being FT-IR analyzed.

2.4 Batch Adsorption Studies

2.4.1 Calibration curves

In a volumetric flask a 0.15985 g of lead nitrate $Pb(NO_3)_2$ (MM= 331.21 g/mol) was dissolved in a 100.0 ml water to produce a stock solution of Pb^{2+} with a concentration of 1000.0 ppm was prepared. By diluting the stock solution we prepared a number of standard Pb^{2+} solutions with concentrations varying from 1.0 ppm to 50 ppm.

Using standard solutions, batch experiments were carried out to investigate the effects of the initial metal ion concentration, contact time, adsorbent dosage, temperature, and pH on the efficiency of the adsorption process.

2.4.2 Calibration curve for lead

By calculating the absorbency of the reference solutions, the calibration curves for Pb^{2+}ions were constructed using flame atomic adsorption spectroscopy (FAAS).

Figure 2.1

The Calibration curve for Pb^{2+}

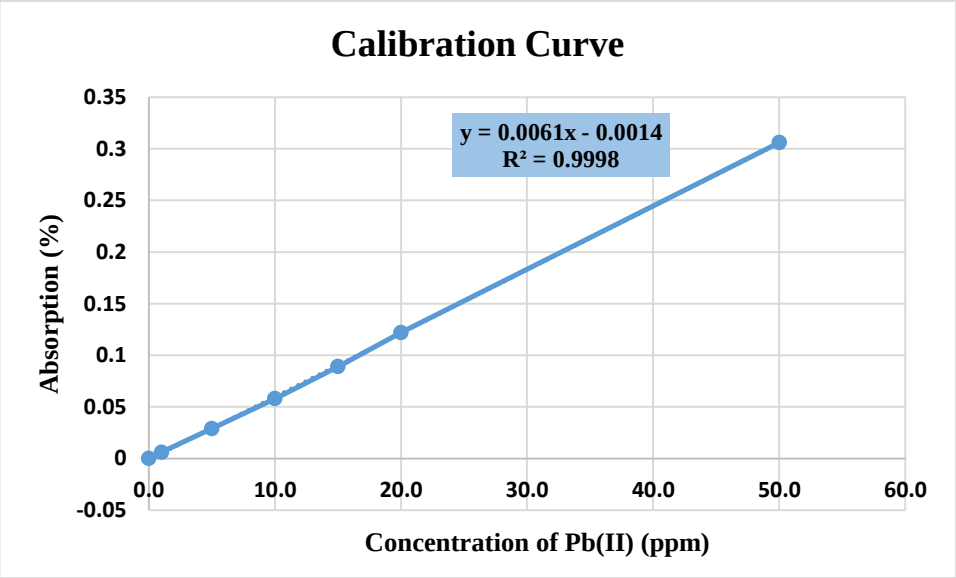

Through batch studies, the removal of Pb^{2+} heavy metal ions from aqueous solutions was investigated [125].

This experiment involved adding a known quantity of polymer to a lead solution with a known concentration in a container, which was then placed in a shaker and submerged in a bath of water. Then, all samples was filtered and analyzed for its residual

concentration. Atomic mass spectroscopy (AAS) was used to determine the concentration of Pb^{2+}.

Also, the equilibrium adsorption capacity (q_e) and removal percentage (E%) were calculated by using equations 2 and 3 shown below [116, 126-130] :

$$q_e = \left(\frac{(C_0 - C_e)}{m}\right) \times V \qquad \textbf{Eq. 2}$$

$$E\% = \left(\frac{(C_0 - C_e)}{C_0}\right) \times 100\% \qquad \textbf{Eq. 3}$$

Where:

q_e : the equilibrium adsorption capacity of the adsorbate (mg/g).

m : the mass of adsorbent (g).

V : the volume of Pb^{2+} solution (L).

C_0 (mg/L) and C_e (mg/L) : the initial and equilibrium concentration of Pb^{2+}, respectively.

2.4.3 The influence of adsorbate (Pb^{2+}) concentration on adsorption percentage

In order to determine the optimum Pb^{2+} ions concentration, five samples we prepared each containing 20.0 mg of adsorbent was mixed with 10 ml of each standard solution (5.0 ppm, 10.0 ppm, 15.0 ppm, 20.0 ppm, and 50.0 ppm). while maintaining the other conditions for the five samples constant (Temp = 25 °C, pH = 4.88, time = 30 min). To examine the remaining lead concentration in each solution, the filtrate of the solution was analyzed by FAAS.

2.4.4 The influence of contact time on adsorption percentage

There were six solutions prepared, each with 10.0 ml of the optimum adsorbate concentration, 10.0 ppm of lead, 20 mg of adsorbent, 25℃, and a pH of 4.88. Thus, all variables were held constant with the exception of the shaking time.

Using a thermostat shaker, the six samples were shaken for 5, 10, 15, 20, 25, and 30 minutes. The filtrate was utilized in the FAAS measurement of the residual lead in each solution.

2.4.5 The influence of polymer dose on adsorption efficiency

In order to study the effect of polymer dosage four samples of Pb^{2+} (10 ml of each) with the optimum concentration of 10.0 ppm and a pH of 4.88 were prepared. Then the polymer was added for each sample with known weights of 10 mg, 15 mg, 20 mg, and 25 mg.

The four samples were shaken using a thermostat mixer at 25 °C for 20 minutes. The remaining lead concentration was determined by filtering all the samples and analyzing the filtrate by FAAS.

2.4.6 The Influence of temperature on adsorption percentage

Four samples were generated in order to examine the impact of temperature on adsorption, each one contains 10 ml form the 10 ppm lead standard solution and loaded with a 20 mg of polymer.

Shaking was done on the samples at various temperatures 15, 20, 25, and 45 ℃ for 20 min, and a pH of 4.88. After the procedure was finished, each solution was filtered out, and the remaining lead in each solution was measured using FAAS.

2.4.7 The influence of pH on adsorption percentage

To investigate the impact of pH, the proper parameters (contact duration, adsorbent dosage, temperature, and standard concentration) were used.

The solutions pH was maintained at 3 to 13. After adding 20 mg of each polymer to 10 ml of a 10 ppm lead standard at 20°C, the samples were purified, and FAAS measured how much lead was still present in each solution.

2.5 Adsorption isotherm

before and after adsorption, the metal ion concentration was measured. Two models, i.e., the Langmuir and Freundlich isotherms were used to measure the distribution of metal ions on the polymer's surface after equilibrium at a constant temperature [131, 132].

The Langmuir model assumes that an adsorbate monolayer would form on an adsorbent surface that is homogeneous.

$$\frac{1}{q_e} = \frac{1}{(Q_{max}\, K_L\, C_e)} + \frac{1}{Q_{max}} \qquad \textbf{Eq .4}$$

Where;

C_e : the ion equilibrium concentration (ppm).

Q_{max} : The adsorbent monolayer adsorption capacity (mg/g).

K_L : The Langmuir affinity constant (L/mg).

The adsorption between the adsorbate molecule and the adsorbent with heterogeneous surface is, nonetheless, described by the Freundlich model.

$$lnq_e = lnK_f + \frac{1}{n} lnC_e \qquad \textbf{Eq .5}$$

Where;

K_f is the Freundlich constant (mg/g).

2.6 Adsorption kinetics

The optimal contact time, pH, It is essential to perform kinetic studies to understand the process by which metal ions are adsorbed and the process pathway.

metal ion concentration, temperature, and polymer dose were used to study the adsorption kinetics.

In 10.0 mL of a Pb^{2+} solution with a concentration of 10.0 ppm, a pH ≈ 7.0, and a temperature range of 20 to 25 °C, about 20 mg of the polymer was added.

The adsorption process has been explained using a variety of kinetic models [133, 134]. One was a pseudo-first order model [135-137]:

$$\ln(q_e - q_t) = lnq_e - K_1 t \qquad \textbf{Eq. 6}$$

The other was pseudo-second order [136, 137] :

$$\frac{t}{q_t} = \frac{1}{(K_2 q^2)} + \left(\frac{t}{q_e}\right) \qquad \textbf{Eq. 7}$$

q_e: mass of adsorbate at equilibrium / mass of adsorbent (mg/g)

q_t: the mass adsorbate/adsorbent mass at time t (mg/g).

K_1 : the first-rate constant (min^{-1}).

K_2 : constant of the second-order rate (g/mg. min).

2.7 Adsorption Thermodynamic

In order to investigated the adsorption performance several thermodynamic parameters it must be taken into consideration such as Gibbs free energy ($\Delta G°$) which demonstrated the spontaneity and feasibility, when ($\Delta G° < 0$) the reaction was spontaneousat a certain temperature, enthalpy ($\Delta H°$), if ($\Delta H° < 0$) the process s exothermic, and entropy ($\Delta S°$) [138, 139].

This parameters were calculated using the following equations [140]:

$$\Delta G° = \Delta H° - T\Delta S° \qquad \textbf{Eq. 8}$$

Where

ΔG° : the change in Gibbs free energy (J/mol).

ΔH° : the change in enthalpy (J/mol).

ΔS° : the change in entropy (KJ/mol.K).

T : the absolute temperature (K).

The relationship between the Gibbs free energy and the equilibrium constant [134, 140]:

$$\Delta G° = -RTlnk_d \qquad (2) \qquad \textbf{Eq.9}$$

R: the universal gas constant (8.314 $J.mol^{-1}. K^{-1}$).

K_d : the thermodynamic equilibrium constant that equals ($\frac{q_e}{Ce}$) with a unit of (mol or L/g).

Substitution of equation 9 into equation 8 [140]:

$$-RTlnk_d = \Delta H° - T\Delta S° \qquad \textbf{Eq. 10}$$

Divided both side by RT [134, 140]:

$$lnk_d = \frac{\Delta S°}{R} - \frac{\Delta H°}{RT} \qquad \textbf{Eq. 11}$$

So plotting $\ln K_d$ against (1/T) in the Van't Hoff plot will give a slope with a gradient of (-ΔH°/R) and an intercept of (ΔS°/R).

It should be noted that the sign of -ΔH° determines whether the gradient is positive or negative. As a result, K increases with temperature in an endothermic reaction while it decreases in an exothermic reaction.

2.8 Wastewater Purification

For this study, in order to evaluate the effectiveness of the polymer produced during the removal of harmful metals from water, a sample of wastewater was taken from one of the Palestinian regions sewage system. One sample was prepared, containing 10 mL of sewage and 20.0 mg of polymer. The polymer was mixed with sewage, and the optimum parameters (temperature, dosage, time, and pH) were selected.

Metal ions in the sample, including their kinds and concentrations, which was compared with a control sample of sewage water, were identified using the ICP-MS technique. (The An-Najah National University's Water Center in Nablus, Palestine, conducted the analysis).

Chapter Three
Results and Discussion

3.1 Polymer Synthesis

3.1.1 Oxidation of cellulose to cellulose$^{-2,3-}$diladehyde (Cell-Ald)

Sodium periodate solution ($NaIO_4$) was used to oxidize cellulose in accordance with a technique created by Jackson and Hudson [141, 142]. It is known that periodate can oxidize an organic compound with vicinal dihydroxyl group to dialdehyde. The reaction conditions and quantity of reagents required to accomplish the oxidation were optimized to obtain highest yield possible of cellulose dialdehyde with high aldehyde content.

In Jackson and Hudson method Periodate ($NaIO_4$) in an aqueous solution is used to treat cellulose in a system that is completely dark. Periodate binds to the adjacent C2 and C3 hydroxyl groups, causing the C2-C3 bond to break and the hydroxyl groups to be oxidized and converted to dialdehyde as shown in **Scheme 3.1** [116, 143, 144].

Scheme 3.1

cellulose is transformed into cellulose-2,3-dialdehyde

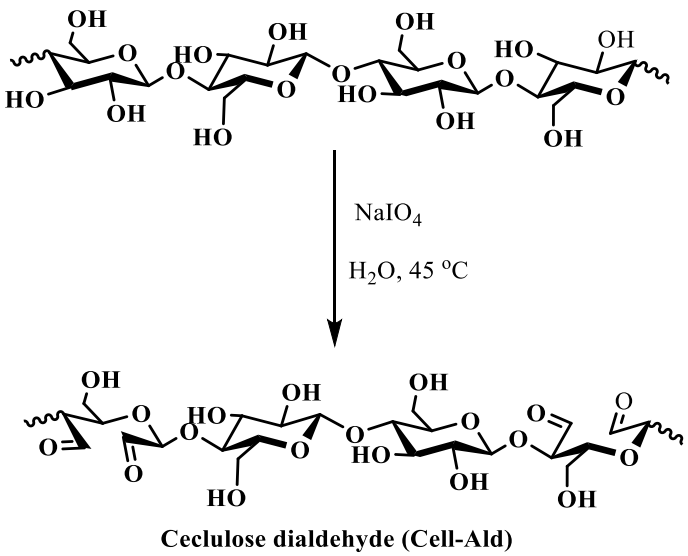

Ceclulose dialdehyde (Cell-Ald)

Note. The image was created to represent mechanism of transformed cellulose to cellulose-2,3-dialdehyde. "by . and احمد .ب.ق, Synthesis of Three Dimensional Cellulose Diamine Polymer for Wastewater Purification. 2018, An-Najah National University." [116].

Scheme 3.2

oxidation of cellulose, reaction mechanism

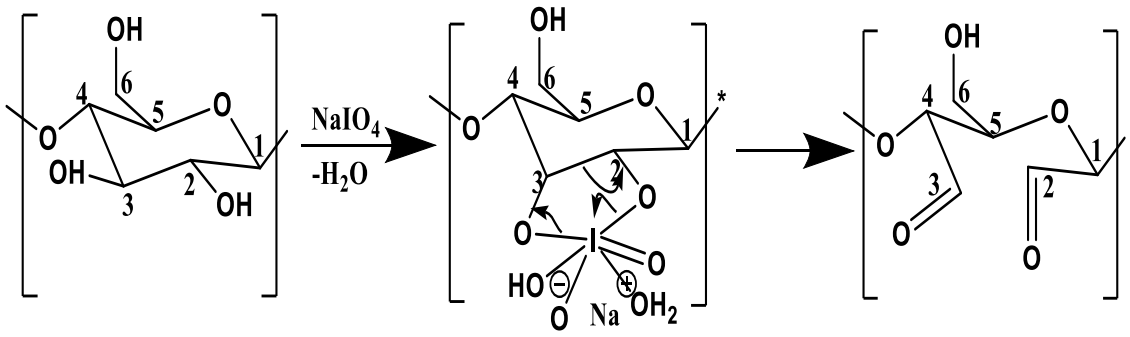

3.1.1.1 Degree of aldehyde substitution

The hydroxylamine hydrochloride method was used to calculate the proportion of aldehyde substitution in the cellulose dialdehyde carried on by the periodate oxidation reaction [116, 124, 130].

In this procedure, a predetermined quantity of dialdehyde cellulose (DAC) was reacted with hydroxylamine-hydrochloride to produce oximes as illustrated in the experimental chapter.

A sodium hydroxide solution with a concentration 0.50 M was used to back titrate the HCl that was released throughout the reaction to an end point of pH 3.50 and the degree of aldehyde substitution was calculated by the following **Eq.12** [116, 130]:

$$[Ald] = \frac{(V_{NaOH} \times N_{NaOH} \times 162)}{W_{OC}} \qquad \textbf{Eq. 12}$$

According to the reaction conditions mentioned in the experimental chapter, the DAC prepared in this work gave a degree of substitution of 1.98 aldehyde group/ anhydro glucose repeat unit of anhydroglucose.

3.1.1.2 Conformation of aldehyde presence by FT-IR

FT-IR spectrum shown in **Figure 3.1** represents the FTIR spectrum of untreated cellulose. The O-H stretching shows a large peak at 3361 cm^{-1}, the band at 2920 cm^{-1} represents the stretching vibration of the C-H bond , peak at 1024 cm^{-1}, associated with C-O-C bond [112, 145].

Figure 3.1

FT-IR spectra of microcrystalline cellulose

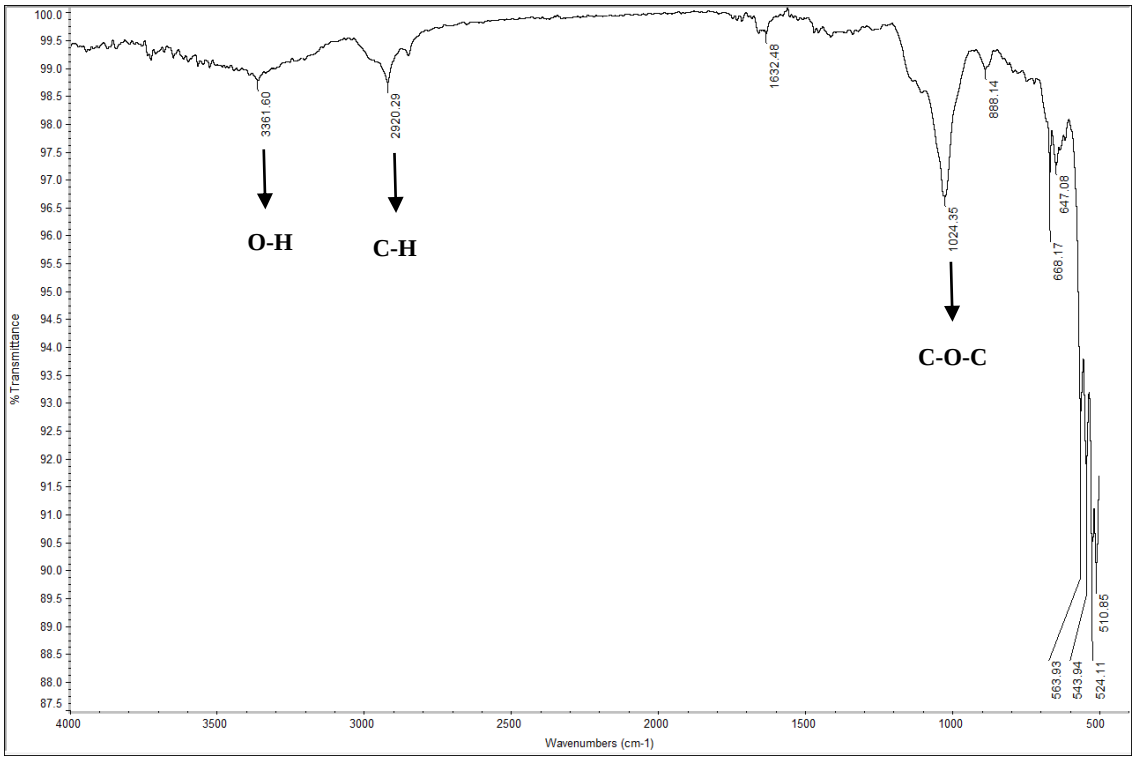

The IR spectrum of the oxidized cellulose **Figure 3.2** exhibits a peak at approximately 1735 cm^{-1} corresponding to the C=O of aldehyde [146]. The absence of a strong aldehyde peak may be caused by hydration and the formation of hemiacetals [147, 148]. Since cellulose had to be dried under extreme temperature in order to remove the water, this could cause aldehyde functional group oxidation or degradation.

Figure 3.2

FT-IR spectra of cellulose after oxidation (Cellulose Dialdehyde)

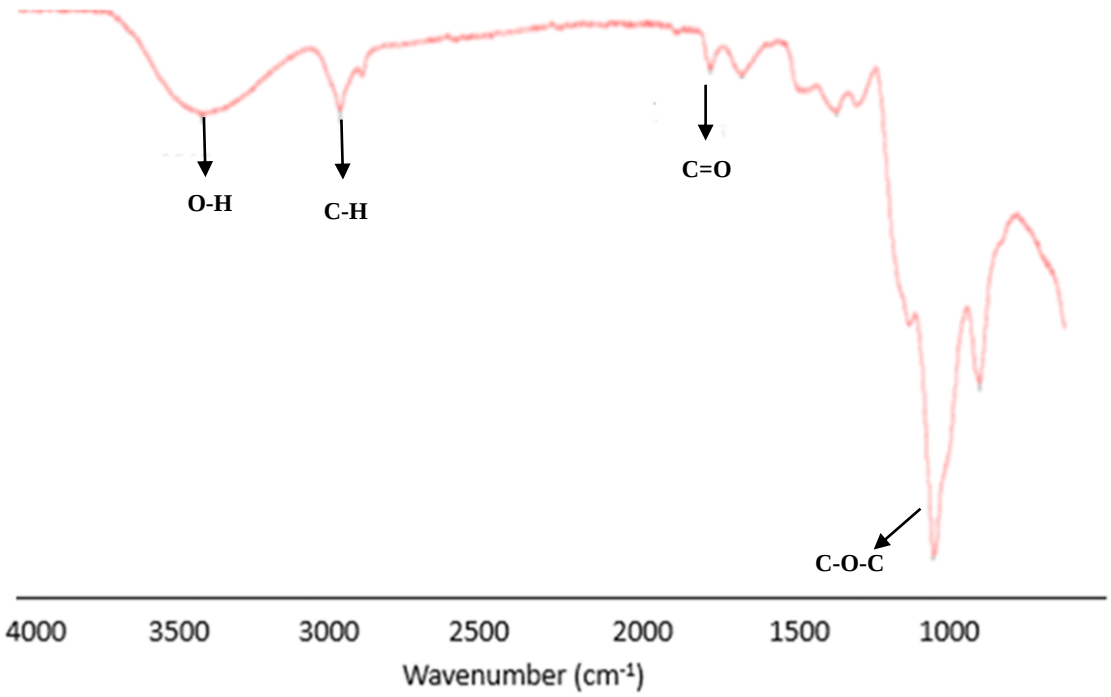

3.1.2 Preparation of Cellulose crosslinked with Diamine

The aldehyde functional group is able to be adapted to many functions or activities [149], It is highly reactive and may be converted into several function groups. It can be undergo further oxidation to form carboxylic groups, for example [150, 151], or reduced to alcohols [150, 152], or converted to imine by reacting it with amine [153]. The imine then could be reduced to an amine. Due to its lone pair of electrons, amine can combine with metal ions. It was transformed to an imine and then reduced to an amine [111, 116].

Aldehyde's carbonyl group contains an electrophilic carbon, after losing the water molecule, the electrophilic carbon reacts with the amine group in a condensation reaction to generate an imine, as shown in **Scheme 3.3** [154].

The scheme shows the reaction between cellulose dialdehyde and *p*-Phenylenediamine. The nucleophilic attachment of an amine to the molecule's carbonyl group first produces an intermediate. Following that, a proton is transferred from nitrogen in PPD to oxygen

in the aldehyde's carbonyl group, and lastly, water is lost in an eliminating reaction to create the imine product.

Scheme 3.3

The transformation of cellulose dialdehyde into cellulose diamine

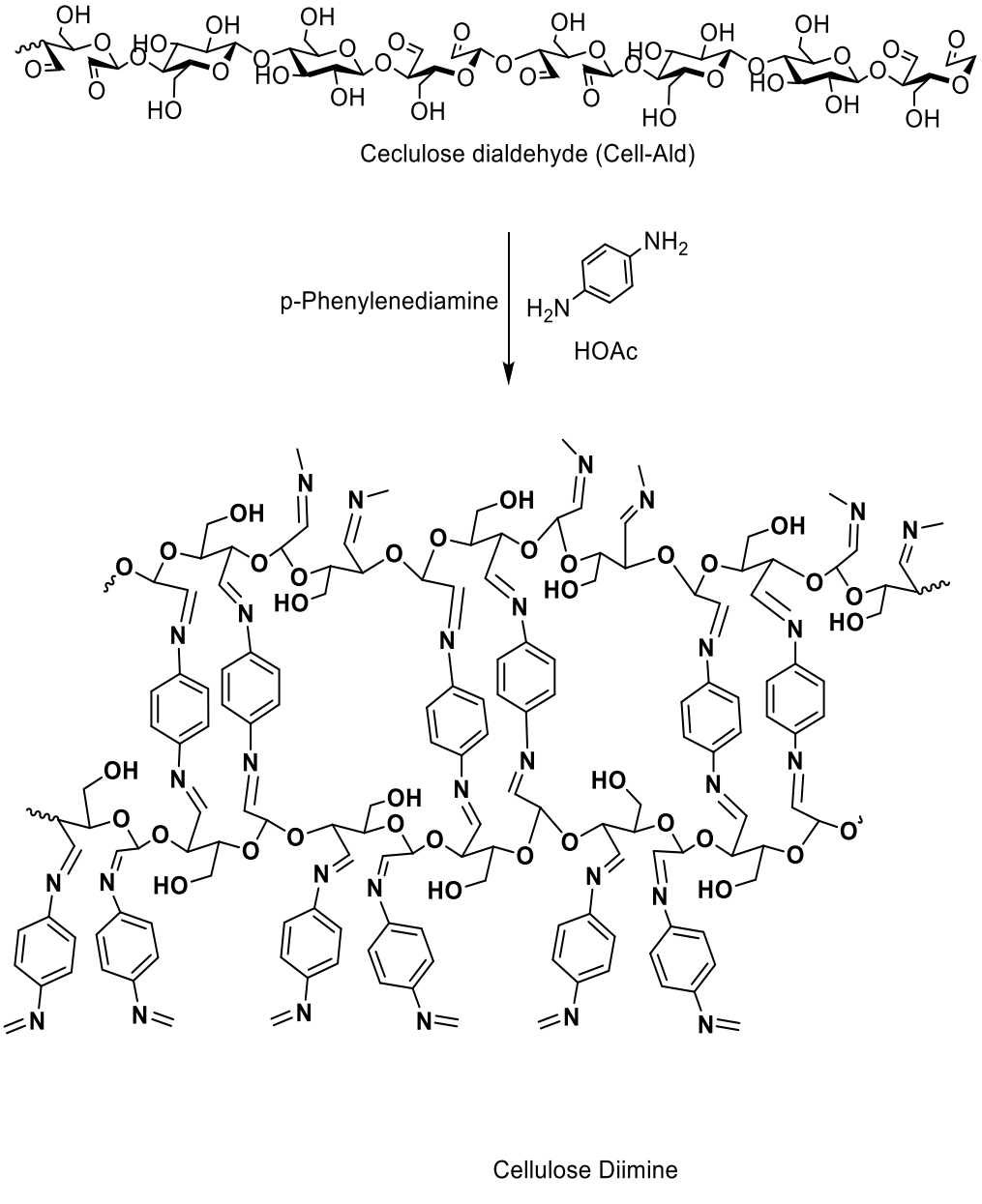

3.1.2.1 FT-IR of cellulose imine

We notice that the aldehyde domain at about 1700 cm^{-1} has disappeared and the appearance of the C=N (imine) at 1632 cm^{-1} and C=C of benzene at 1513 cm^{-1}, also we noticed that the appearance of C-N at about 1260 cm^{-1} and at 3358 cm^{-1} is the stretching of the O-H group. (**Figure 3.3).**

Figure 3.3

FT-IR spectra of Cellulose Diimine.

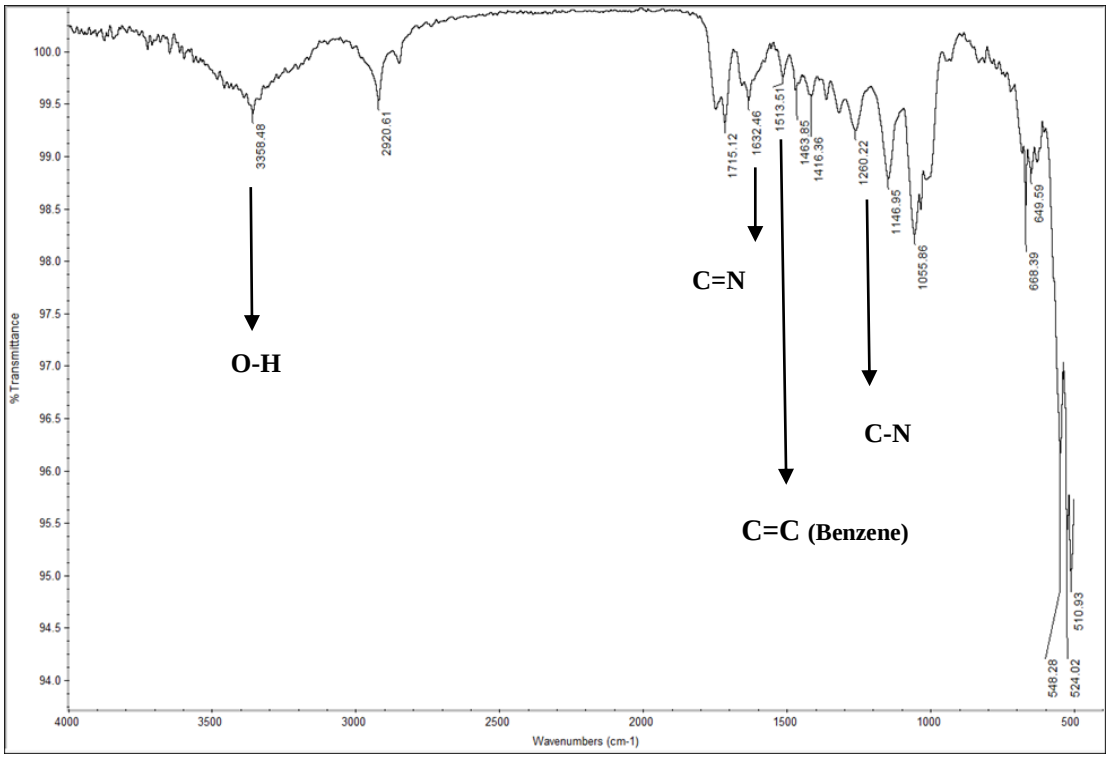

3.1.3 Conversion of Cellulose Diimine to a cellulose Diamine by Reduction

Sodium borohydride was used to reduce cellulose imine, the reaction usually takes place in methanol, and it is a direct forwarded reaction **Scheme 3.4**.

PPD was chosen because it forms a crown amine with a strong affinity for metal when it crosslinks to the cellulose chains.

Scheme 3.4

Reduction of Cellulose Diimine to cellulose Diamine

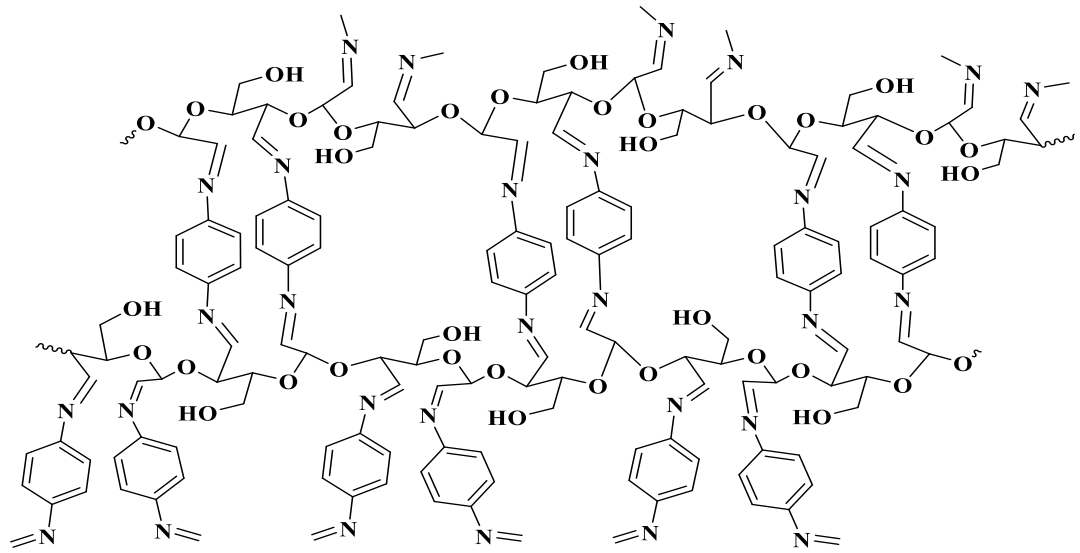

Cellulose Diimine

$NaBH_4$

MeOH

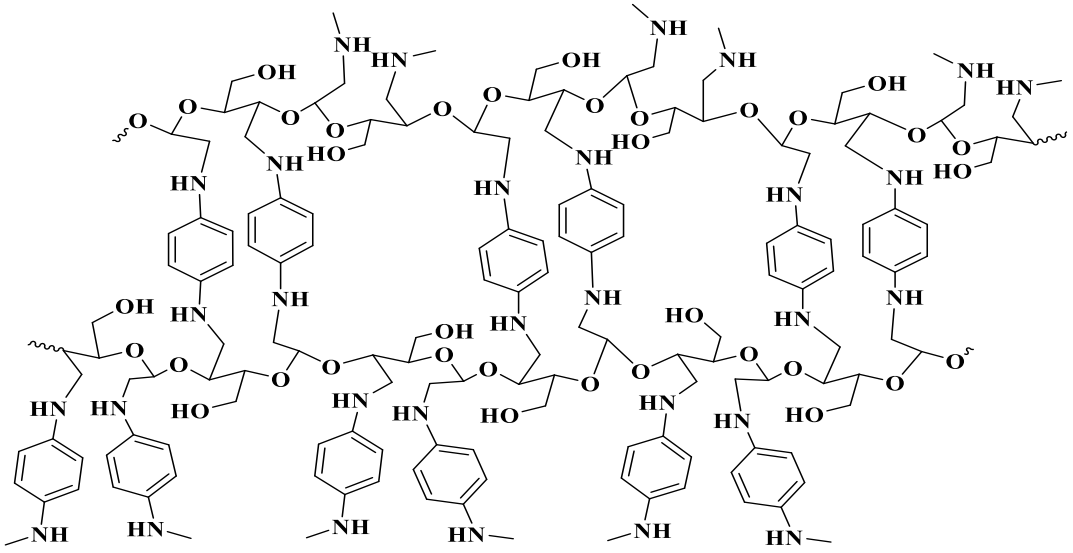

Cellulose Diamine

3.1.3.1 FT-IR of cellulose diamine

The disappearance of the imine band at 1675 cm is clear in **Figure.3.4** of the obtained FT-IR spectra. aromatic rings containing C=C is detected by a signal at 1595 cm^{-1}. The N-H band emerged at approximately 3376 cm^{-1}, but it was discovered that when the imine groups were changed into amines, the signal size increased, and this region also shows the O-H band, which. As a result, the signal appears to be somewhat broader.

Figure 3.4

FT-IR Spectra of Cellulose crosslinking with amine.

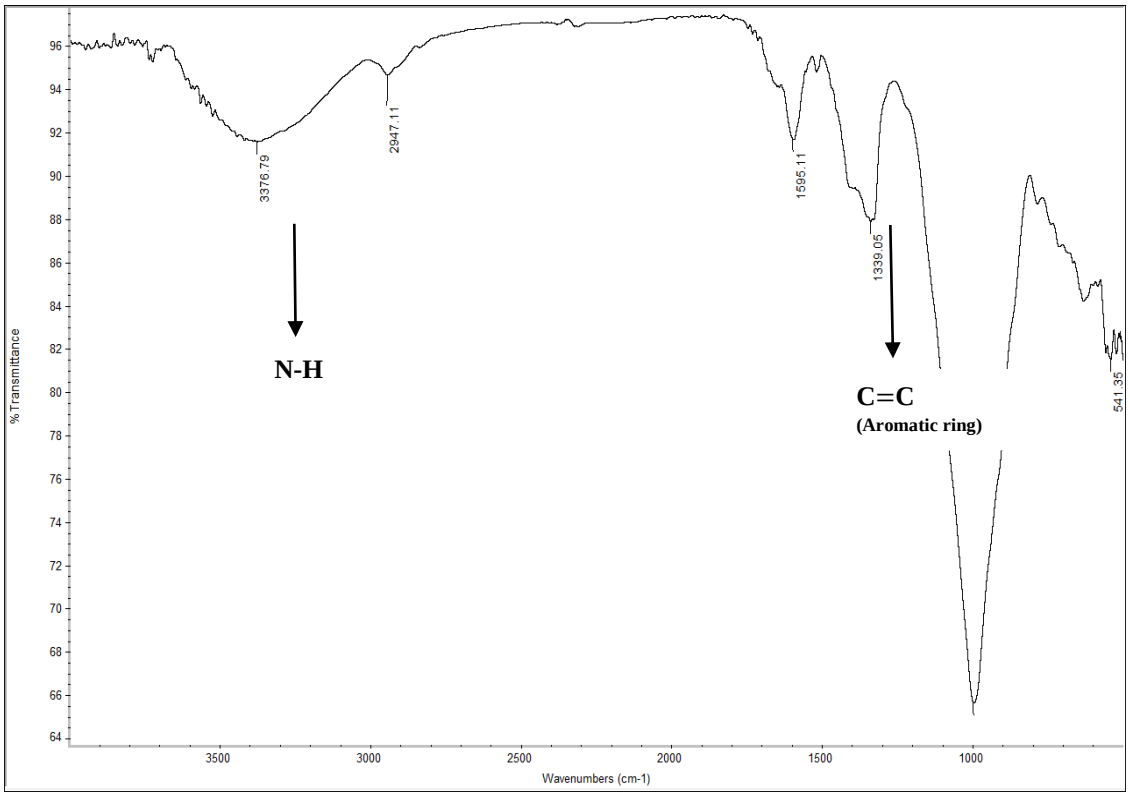

3.1.4 Preparation of Cellulose with Zwitterionic functionality

In the last step, cross-linked cellulose will be reacted with 1,3-propane sultone. The cyclic sulfonate undergoes ring opining addition reaction with the amine group in the crosslinked cellulose to form the target cellulose with zwitterionic functionality (Cell-X-ZWC) **Scheme 3.5** [64, 81, 155, 156].

Scheme 3.5

Conversion of crosslinked Cell-Ald to cellulose based zwitterionic

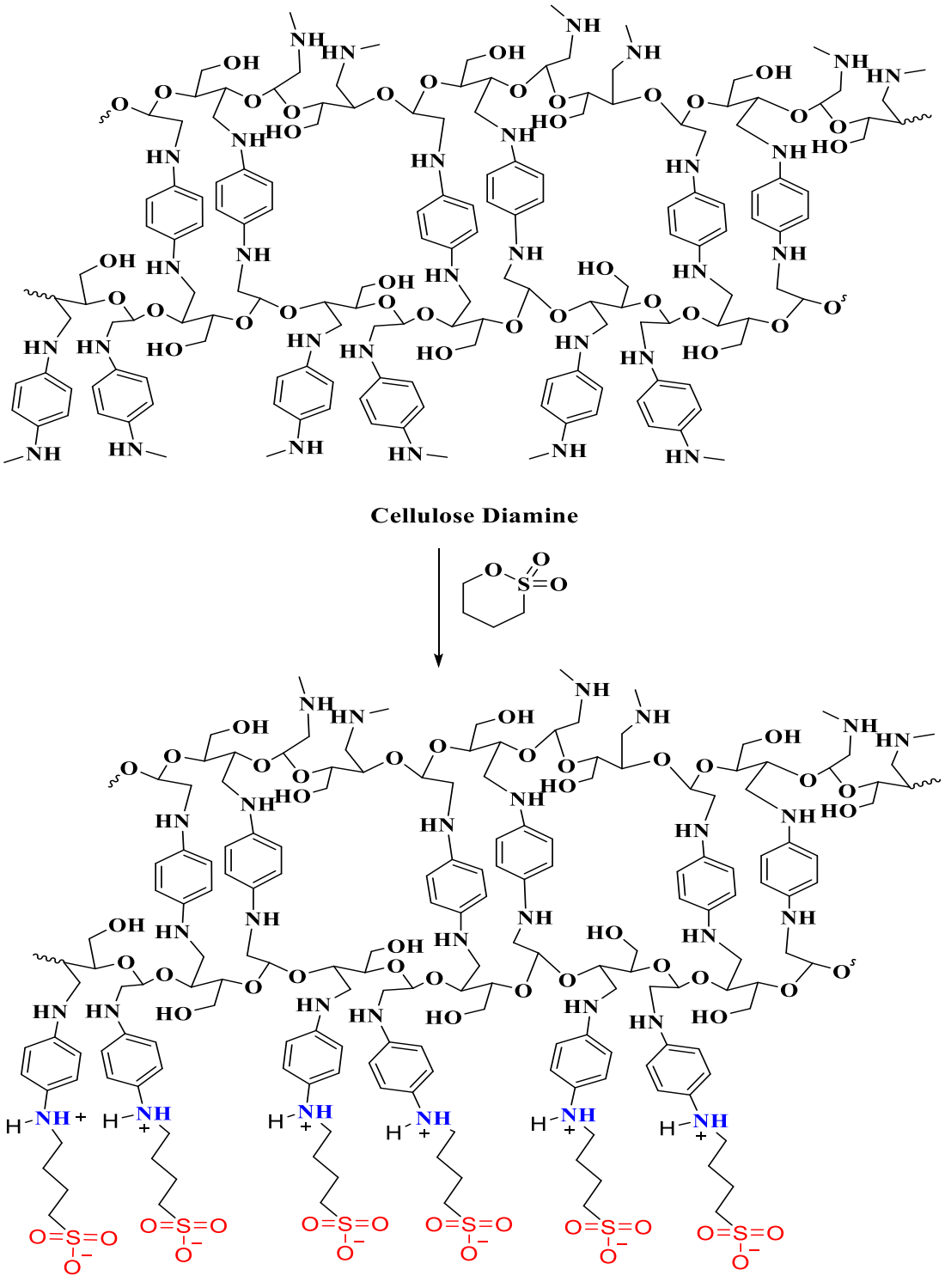

Cellulose Diamine

Cellulose with zwitterionic functionality (Cell-X-ZWC).

3.1.4.1 FT-IR of Cellulose based zwitterionic.

The C-H stretching peaks at 2901 and 2960 cm^{-1} are more intense than usual indicating the presence of long alkyl chain represented by butyl group. The band at 1229 cm^{-1} represents the sulfonate group.

Figure 3.5

IR spectra of Cell-X-ZWC

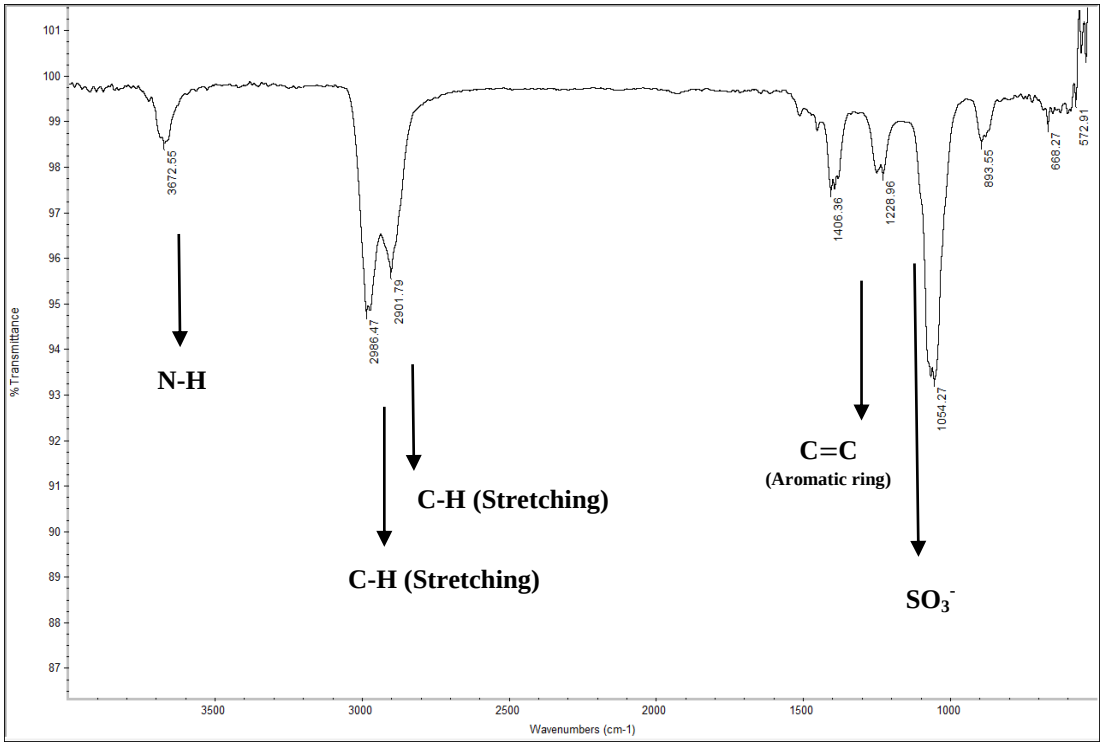

3.2 Adsorption of Pb (II)

One of the main goals of this study is to utilize Cell-X-ZWC for the removal of hazardous, heavy metals from industrial wastewater. This procedure was carried out by examining the adsorption efficiency of the prepared polymers (Cell-X-ZWC) to adsorb Pb^{2+} ions. According to **section 2.4**.

The procedure was done by investigating the removal capabilities of PPD towards Pb^{2+}. Atomic adsorption spectroscopy was used to calculate the remained heavy metal ion concentrations. the percentage of removal was determined using Eq.13 [157].

$$\%Adsorption = \left(C_i - \frac{C_f}{C_i}\right) \times 100\% \qquad \textbf{Eq.13}$$

Where;

C_i : zero time concentration of metal ion in solution (ppm).

C_f : Concertation of metal ion after the adsorption (ppm).

Under experimental conditions, qe (mg/g) is the adsorption capacity determined for various concentrations of ions at equilibrium [158].

$$q_e = \left(\frac{(C_0 - C_e)}{m}\right) \times V \qquad \textbf{Eq.14}$$

where;

m: the mass of adsorbent (g).

V: the volume of Pb^{2+} solution (L).

C_0 : concentration of metal ion in solution at time zero (ppm).

C_e : Concertation of metal ion after the adsorption (ppm).

3.2.1 Adsorption of Lead Ions (Pb2+)

3.2.1.1 The influence of Pb2+ Initial Concentration

This was done to evaluate how the concentration of metal ions affected the rate of Pb^{2+} metal ions removal from solutions. Lead solutions with a various concentration and 20.0 mg of polymer was used.

The other parameters (temperature, pH, shaking time, and solution volume) were set at 25 °C, 4.88, 30 minutes, and 10.00 ml according to experimental part **sec. 2.4.3.**

Table 3.1 shows the result obtained for the effect of the concentration of adsorbent on the adsorption of Pb^{2+} ions.

Table 3.1

Effect of adsorbate concentrations on Pb^{2+} ions adsorption

Initial concentration of Pb^{2+} (ppm)	Final concentration of Pb^{2+} (ppm)	Adsorption (%)	Residual (%)	Q_e (mg/g)
5.0	0.56	88.79	11.21	2.22
10.0	0.91	90.90	9.10	4.55
15.0	3.60	76.00	24.00	5.69
20.0	6.81	65.94	34.06	6.59
50.0	18.27	63.47	36.53	15.87

The adsorption capacity and removal percentage as a function of initial adsorbate concentration are shown in **Figure 3.6 (in appendix B).**

As **Figure 3.6 (a) (in appendix B)** shows, a proportional relationship was noticed between Pb^{2+} ion concentration and the %adsorption. The percent adsorption increase with increasing the initial concentration and reaching a maximum percentage when the initial concentration reached 10.0 ppm, then started to decline, and becomes steady at a concertation over 20 ppm the maximum percent of removal was 90.90 %.

As lead ions concentrations increases as long as vacant sites are available, the rate of adsorption declines when the vacant sites become occupied [100].

Most lead ions were adsorbed into the polymer mass at low lead concentrations and bound to the active sites, where they remained until all the active sites were occupied. The absorption process reaches a peak at 10 ppm. Following this concentration, the surface layer is covered with Pb^{2+} and this limits the adsorption process and stop the absorption of further lead ions [100].

Figure 3.6 (b) (in appendix B) shows the relation between the initial concentration of adsorbate and the adsorption performance. The high driving force of the mass transfer and the abundance of unoccupied receipting sites [40].

The adsorption capacity initially rises quickly as the adsorbate concentration rises until it reaches a plateau, at which point it can be concluded that all of the adsorption sites have been occupied [40].

3.2.1.2 Influence of contact time

Removal of lead as a function of time was studied under optimum initial ions concentration 10.00 ppm, and other parameters such as pH, temperature, dosage volume of adsorbate (4.88, 25 ℃, 20.0 mg, 10 ml) were kept constant. The effect of adsoprtion time on Pb^{2+} removal was studied using contact time values that ranged from 5-30 minutes. The influence of contact time on adsorption percentage are presented in **Table 3.2.**

Table 3.2

Effect of the contact time on Pb^{2+} ions adsorption

Contact time (min)	**Initial concentration of Pb^{2+} (ppm)**	**Final concentration of Pb^{2+} (ppm)**	**Adsorption (%)**	**Residual (%)**	**Q_e (mg/g)**
5 min	10.0	3.07	69.26	30.74	3.46
10 min	10.0	1.44	85.58	14.42	4.28
15 min	10.0	1.53	84.69	15.31	4.23
20 min	10.0	1.34	86.59	13.42	4.33
25 min	10.0	1.78	82.22	17.78	4.11
30 min	10.0	1.62	83.77	16.23	4.19

As shown in **Figure 3.7 (a) (in appendix B)**, From 5 to 15 minutes, the removal percentage was gradually increased; after that, it nearly remained constant. The optimum contact time was chosen to be the one that typically results in the lowest residual concentration of adsorbate.

The results shown in **Figure 3.7** indicate that the optimum adsorption performance occurred at 20 minutes with 86.59 % removal for Pb^{2+}, when all active sites were filled. As a result, minimal adsorption occurred when the contact time was short because there was insufficient energy to drive lead ions into the polymer's pores. Better %adsorption was achieved as a result of the lead ions adsorbed more quickly when the contact time was increased because they were easily dispersed to the pores and surface [159].

Contact time is another crucial factor to consider when evaluating how favorable the adsorption process is. The short time to reach adsorption equilibrium suggests that

larger treatment volumes or batches can be treated in a low time interval, increasing removal effectiveness and lowering water treatment system costs [40].

The presence of abundance vacant binding sites on the adsorbent surface causes the adsorption capacity often increases quickly during the first contact period. The rise in adsorption capacity gradually decreases until it levels off, indicating that the adsorption equilibrium has been achieved [40, 160].

This is because as contact time increases, the number of vacant adsorptive sites decreases and collision between the adsorbate and adsorption sites meet much higher resistance [40, 160].

Figure 3.7 (b) (in appendix B) displays a plot of adsorption capacity versus contact time variation. The plot indicates that the adsorption capacity is initially greatly enhanced and then gradually decreases over the period of 10 minutes. After 20 minutes, adsorption stopped and reached equilibrium [160].

3.2.1.3 Influence of Adsorbent Dosage

The influence of adsorbent dosage on Pb^{2+} removal process was essential to study since it relates to the amount of available active state. To determine the optimum quantity of adsorbent Cell-X-ZWC that gave the best and highest adsorption percentage, the solutions concentration, and the contact time were set at, 10 ppm, and 20 minutes, respectively.

Other parameters such as temperature, volume, and pH were kept constant, 25℃, 10 ml, and 4.88, respectively.

The highest removal was obtained at the addition of 20 mg adsorbent for Pb^{2+} removing. The results are presented in **Table 3.3.**

Table 3.3

Effect of the adsorbent dosage on Pb^{2+} ions adsorption

Polymer dosage (mg)	Initial concentration of Pb^{2+} (ppm)	Final concentration of Pb^{2+} (ppm)	Adsorption (%)	Residual (%)	Q_e (mg/g)
10	10.0	4.54	54.63	45.37	2.73
15	10.0	3.66	63.36	36.64	3.17
20	10.0	1.23	87.72	12.28	4.39
25	10.0	1.56	84.39	15.61	4.22

As shown in the above figure (**Figure 3.8(a)) (in appendix B),** as the adsorbent dose increases, the absorption percentage increases, which could be related to the availability of abundant vacant sites until it reaches maximum indicating the reaching of the adsorption equilibrium, after that the removal percentage declines as the dosage increases, due to the limited total available sites. The adsorption percentage was higher at 20 mg with 87.72 % removal for Pb^{2+}, so 20 mg was the optimum adsorbent dosage [40, 161].

Adsorbent dosage (mg) is an important factor in estimating adsorption capacity and removal efficiency.

Figure 3.8(b) (in appendix B), illustrates a typical relationship between adsorption performance and adsorbent dosage.

Due to the abundance of unoccupied binding sites, the adsorption capacity increases rapidly with an increase in adsorbent dosage before gradually plateauing as a result of the saturation of adsorption sites on the adsorbent surface.

Similarly, **Figure 3.8(b)** illustrates how an excessive increase in adsorbent decreases adsorption capacity by increasing the number of vacant binding sites. Another reason for the decline in adsorption capacity could be the possibility of particle aggregation at high concertation of adsorbent, which results in a drop in the adsorbent's total surface area [162, 163].

3.2.1.4 Influence of Temperature

The optimum values for dosage, concentration, contact time, and pH were constant at 20.0 mg, 10.00 ppm, 20.00 min, and 4.88, respectively, to study the impact of temperature on Pb^{2+} ions adsorption utilizing Cell-X-ZWC which ranged from (15 - 45)°C **(sec.2.4.6).** The results are presented in **Table 3.4** and **Figure 3.9(in appendix B)** summarized the results.

Table 3.4

Effect of the temperature on the adsorption of Pb^{2+} ions

Temperature (℃)	**Initial concntration of Pb^{2+} (ppm)**	**final concntration of Pb^{2+} (ppm)**	**Adsorption (%)**	**Residual (%)**	**Q_e (mg/g)**
15	10	1.42	85.79	14.21	4.29
20	10	1.19	88.09	11.90	4.40
25	10	1.28	87.20	12.80	4.36
45	10	2.47	75.32	24.68	3.77

Temperature is another crucial factor since it can affect the activation energy of the adsorption system, which in significantly influence the removal rate and adsorption capacity.

When the effectiveness of the adsorption is improved by raising the temperature, this process should be endothermic; otherwise, it should be exothermic [164].

In the endothermic process the adsorption capacity and removal rate are increased by rising the temperatures because of the increasing rate of effective collision (with enough energy to surpass the activation energy) between the metal ion and the adsorption sites on the adsorbent surface [165].

Figure 3.9 (a) (in appendix B) shows that adsorption decreased as temperature increased, the maximum removal percentage can be achieved at 20 ℃, with removal of 88.096%, so it is the optimum temperature. However, the rate of Pb^{2+} ion removal decreases as the temperature rises from 25°C to 45°C, showing that neither cooling nor heating the solution is required to adsorb the metal ion.

From the **Figure 3.9 (b) (in appendix B)** it can be observed that the effect of increasing the temperature is to decrease the adsorption capacity.

The results showed that the exothermic and spontaneous character of Cell-X-ZWC adsorption processes. The kinetic energy of the adsorbed particles rises with temperature, increasing the probability that they will separate from the adsorbent surface [166, 167]. Furthermore, the decrease in adsorption at higher temperatures may be the cause of the increase in ion solubility with temperature [168].

3.2.1.5 Influence of pH on rate of adsorption

The pH of the metal ion solution is a crucial factor in controlling the metal removal process because it influenced the binding site for heavy metals. the optimized experimental conditions were held constant (10.00 ppm solution concentration, 20.00 min, contact time, temperature 20 ℃, and Cell-X-ZWC,20.00 mg.

As mentioned in the experimental section, the effect of pH on the polymer's capacity for adsorption was investigated **(sec. 2.4.7). Table 3.5** presents the results about the effect of pH value on Pb^{2+} ions adsorption.

Table 3.5

Effect of pH level on Pb^{2+} ions adsorption

pH	Initial concntration of Pb^{2+} (ppm)	Final concentration of Pb^{2+} (ppm)	Adsorption (%)	Residual (%)	Q_e (mg/g)
3.53	10.0	0.56	94.40	5.61	4.72
5.48	10.0	0.33	96.69	3.31	4.83
7.21	10.0	0.12	98.77	1.23	4.94
9.14	10.0	0.19	98.15	1.86	4.91
11.38	10.0	0.49	95.11	4.89	4.76

Figure 3.10(in appendix B) illustrates the results using a range of pH values, from basic mediums with a pH of 11.38 to acidic mediums with a pH of 3.53.

From **Figure 3.10 (a) (in appendix B)**, the maximum adsorption for Pb^{2+} ions occurred at a pH of ≈ 7.21. pH value increased, adsorption increased up and reached the highest at pH ≈ 7.21 then decreased which means prefers acidic medium over alkaline one.

Transfer to basic medium decrease the adsorption. Likewise in the **Figure 3.10 (b) (in appendix B)** the adsorption capacity increases as the pH value increases until it reaches a plateau at pH ≈ 7.21 then the adsorption capacity decreased in alkaline medium pH >7.21.

The fact that metal oxide starts to form at higher pH values can be used to explain the decreasing behavior of the Pb^{2+} removal ratio and adsorption capacity after the polymer's optimal pH [169].

3.3 Optimum adsorption parameters

The optimum adsorption parameters for Pb^{2+} ions are shown in **Table 3.6.**

Table 3.6

Optimum Adsorption Parameters for lead ions

Adsorbent	Metal ion	%Adsorption	Parameters dosage (mg), concentration (ppm), Contact time (min), Temp (°C), pH
Cell-X-ZWC	Pb^{2+}	97.43%	20mg, 10ppm, 20min, 20℃, ≈7.21

3.4 Adsorption analysis

3.4.1 Adsorption Isotherm

To examine the produced polymer adsorption equilibrium effectiveness (cellulose-based polumer) in removing Pb^{2+} ions, at equilibrium. The Langmuir (**Eq. 15**) and Freundlich (**Eq. 16**) isotherms models were utilized [132, 170, 171].

Once equilibrium was achieved under constant temperature, both adsorption isotherm models were used to assess the adsorbate spreading on the surface of the adsorbent [112].

There are several isotherm models that apply at all temperatures, including Langmuir, Freundlich, and others. When the ions are arranged in a monolayer on the surface of the adsorbent, the Langmuir model guides the adsorption process.

The Freundlich model is used when the adsorption process between the adsorbent and the adsorbate is conducted on a large number of heterogeneous layers [171].

These models all have applicable equations, and the data will be fitted into these equations. The correlation coefficients, R^2, are one of the factors that can influence the sort of isotherm model [112, 170].

3.4.1.1 Langmuir adsorption isotherm

The fundamental principles of the Langmuir model are a finite number of active sites that are homogenously distributed over the adsorbent's surface, Monolayer adsorption and desorption on one active center have no impact on the adsorption on another active center because all active centers have the exact same level of energy [172-176].

The adsorption follows this model if the figure plot between $1/q_e$ vs $1/c_e$ shows a straight line with a high R^2 value. It was presented as **Eq .15**:

$$\frac{1}{q_e} = \frac{1}{(Q_{max}\, K_L\, C_e)} + \frac{1}{Q_{max}} \qquad \textbf{Eq .15}$$

Where;

C_e : the ion equilibrium concentration (ppm).

At equilibrium, q_e is the mass of the adsorbate that is absorbed per mass of the polymer (mg/g).

Q_{max} : The adsorbent's monolayer adsorption capacity (mg/g).

K_L : The Langmuir affinity constant (L/mg) that is related to the adsorption energy.

The separation factor (R_L), also known as the equilibrium parameter, is a dimensionless constant that can be used to characterize the basic characteristics of the Langmuir isotherm [175, 177].

$$R_L = \frac{1}{1+K_L C_0} = 1 + \frac{1}{K_L C_0} \qquad \textbf{Eq .16}$$

Where

C_0 : is the initial concentration (mg/L).

K_L : is the Langmuir constant related to the energy of adsorption (L/mg).

The value of R_L indicates the shape of the isotherms to be either unfavourable ($R_L > 1$), linear ($R_L = 1$), favourable ($0 < R_L < 1$) or irreversible ($R_L = 0$).

Figure 3.11 (in appendix B) Represent Langmuir model for adsorption of Pb^{2+} on Cell-X-ZWC.

Table 3.7

Langmuir model values

Concentration (ppm) C_i	**$[Pb^{2+}]$ (ppm) C_e**	**q_e**	**$1/C_e$**	**$1/q_e$**
5	0.56	2.22	1.78	0.45
10	0.91	4.55	1.09	0.22
15	3.60	5.69	0.28	0.18
20	6.81	6.59	0.15	0.15
50	18.27	15.87	0.05	0.06

Table 3.8

Langmuir Adsorption isotherms parameters for Cell-X-ZWC

		Langmuir isotherms			
Metal ion	**Adsorbent**	**R^2**	**Q_{max}**	**K_L**	**R_L**
Pb^{2+}	Cell-X-ZWC	0.88	11.16	0.49	0.17

As shown on **Table 3.8**, the separation factor (R_L) range from ($0 < R_L < 1$) which indicates that the shape of the isotherms is favorable. This replicates the strong attraction that the polymers made of cellulose have for the investigated metal ions.

3.4.1.2 Freundlich isotherm model

The adsorption processes on heterogeneous surfaces with a non- uniform distribution of energy of adsorption and multilayer adsorption are discussed and illustrated in the Freundlich isotherm model.

If the graph of $\ln q_e$ versus $\ln C_e$ displays a straight line with an R^2 number close to 1, then adsorption follows to this model.

The Freundlich isotherm has the following empirical formula:

$$lnq_e = lnK_f + \frac{1}{n} lnC_e \qquad \textbf{Eq .17}$$

Where;

K_f is the Freundlich constant, which is proportional with the adsorption capacity (mg/g).

The heterogeneity coefficient (g/L) is denoted by the letter n, which indicate how favorable or unfavorable the adsorption process (g/L).

Figure 3.12 (in appendix B) represent Freundlich model for adsorption of Pb^{2+} by Cell-X-ZWC.

Table 3.9

Freundlich model values

Concentration (ppm) C_i	**$[Pb^{2+}]$ (ppm) C_e**	**q_e**	**$\ln q_e$**	**$\ln C_e$**
5	0.56	2.22	0.79	-0.58
10	0.91	4.55	1.51	-0.09
15	3.60	5.69	1.74	1.28
20	6.81	6.59	1.89	1.92
50	18.27	15.87	2.76	2.91

Table 3.10

Freundlich Adsorption Isotherms parameters for Cell-X-ZWC

		Freundlich isotherms		
Metal ion	**Adsorbent**	**R^2**	**n**	**K_f**
Pb^{2+}	Cell-X-ZWC	0.89	2.15	3.44

In all cases, as show in **Table 3.8 and Table 3.10,** Compared to the Langmuir isothermal model, the Freundlich isothermal model's correlation coefficient (R^2) is higher and much closer to 1.

So, the adsorbent (Cell-X-ZWC) obeys this model and adsorption process is not only at the surface, but also at the multilayer of the polymer, and adsorption processes on heterogonous surfaces.

3.4.2 Adsorption kinetics

One of the major features that must be understood before any adsorbent can be applied is adsorption kinetics [162].

In order to examine the adsorption process involves rate of adsorption and mechanism of adsorption of Pb^{2+} the kinetic models pseudo-first order and pseudo-second order were utilized. The employed kinetic models are shown in **Eqs. 18 and 19** [178-180].

3.4.2.1 Pseudo-first order model

$$\ln(q_e - q_t) = lnq_e - K_1 t \qquad \textbf{Eq. 18}$$

where;

K_1: the first-order rate constant (min^{-1}).

q_e: the equilibrium amount of solute adsorbed per unit weight of adsorbent (mg/g).

q_t: the amount of solute adsorbed per unit weight of adsorbent at any given time (mg/g).

If the graph of $\ln(q_e-q_t)$ vs. time displays a straight line with a high R^2 value, the adsorption follows this model.

Table 3.11 (in appendix A) shows Values of the pseudo-first order model.

Table 3.12 (in appendix A) represents Adsorption kinetic parameters for the adsorption of Pb^{2+} on Cell-X-ZWC (pseudo-first order model).

Figure 3.13 (in appendix B) represents pseudo-first order model for Pb^{2+} absorption on Cell-X-ZWC.

3.4.2.2 Pseudo-second order

Is based on the solid phase's adsorption capacity and is represented as:

$$\frac{t}{q_t} = \frac{1}{(K_2 q^2)} + \left(\frac{t}{q_e}\right) \qquad \textbf{Eq .19}$$

where;

K_2 : the second-order rate constant (g mg^{-1} min^{-1})

q_e : the equilibrium amount of solute adsorbed per unit weight of adsorbent.

q_t : the amount of solute adsorbed per unit weight of adsorbent at any given time.

If the plot of t/q_t vs. time exhibits a straight line with an R^2 value approaching 1, the adsorption will follow to this model.

Table 3.13 (in appendix A) shows Pseudo-second order model values.

Table 3.14 (in appendix A) represents Adsorption kinetic parameters for the adsorption of Pb^{2+} on Cell-X-ZWC (pseudo-second order model).

Figure 3.14 (in appendix B) represents Pb^{2+} absorption on Cell-X-ZWC: pseudo-second order model.

From the correlation coefficients (R^2) of pseudo-first and second order, it is clear that the adsorption of lead ions on Cell-X-ZWC follows pseudo-second order because in this case (R^2=0.99) is higher than (R^2 = 0.18) obtained in the first order.

The fact that the theoretical q_e value for the pseudo-second order model (4.28 mg/g) is so close to the experimental q_e value (4.55 mg/g) also suggests that the process of Pb^{2+} adsorption on the surface of the cellulose polymer conforms to the pseudo-second order.

3.4.2.3 Intra-particle diffusion Weber-Morris model

The metal removal process by adsorption typically consists of several stages the first step involves transfer of metal ions from the the solution to the outer surface of the Cell-X-ZWC polymer. Then diffuse of ions to the outer surface of the Cell-X-ZWC polymer across the boundary layer, then metal ion adsorption at active sites on the surface of Cell-X-ZWC polymer occurs, and in the last stage involves ion adsorption and intraparticle diffusion to the inner sites of particles of Cell-X-ZWC polymer[112, 176].

In this works, the intraparticle diffusion model and the liquid film model were used to study the sorption mechanism.

Using the Morris-Weber equation, the intra-particle diffusion model can be constructed. The model shows a linear correlation between the quantity adsorbed (q_t) and the square root of the time.

The rate-determining step of metal ion adsorption onto Cell-X-ZWC was determined using the intraparticle diffusion model described in **Eq. 20** [181].

$$Q_t = K_{id} t^{\frac{1}{2}} + Z \qquad \textbf{Eq .20}$$

Where;

Q_t : are adsorption capacities (mg/g) at various time (t,min).

K_{id} : is the intraparticle diffusion rate constant (mg/g $min^{1/2}$)

Z : (mg/g) the thickness of the boundary layer.

Table 3.15 (in appendix A) shows Intraparticle diffusion model values.

Table 3.16 (in appendix A) represents Kinetic adsorption parameters (Intraparticle diffusion model) for the adsorption of Pb^{2+} on Cell-X-ZWC.

Figure 3.15 (in appendix B) represents Intraparticle diffusion model of Pb^{2+} adsorption by Cell-X-ZWC.

The values of K_{id} and Z were determined using **Figures 3.14** (Q_t vs. $t^{1/2}$). The values are summarized in **Table 3.16**. Each plot in **Figures 3.13** and **3.14** was linear and didn't pass through the origin, showing that more than one rate-limiting steps take place.

The external surface adsorption stage, also known as the instant adsorption stage, is the first, sharper part. The steady adsorption step, which is the second part (intraparticle diffusion) is the rate-controlled. In the third section, which is the last equilibrium stage, intraparticle diffusion begins to slow down as a result of extremely low adsorbate concentrations in the solution [182].

The values of Z (**Table 3.16**) show an increase in the potential for internal mass transfer, a decrease in external mass transfer and an expansion of the outer layer [112, 132, 183].

The linearized intraparticle diffusion model is presented at each concentration under consideration in **Figure 3.15.** The external surface adsorption (stage 1) is not present, as seen in **Figure 3.15.** Stage 1 is completed before 3 min, stage 2 (intraparticle diffusion control) is attained and continues from 3 min to 10 min. Finally, after 10 minutes, stage 3 of final equilibrium adsorption begins.

Through intraparticle diffusion, the lead is slowly absorbed by the particles and then retained in the micropores. Generally, the intraparticle diffusion rate constant, abbreviated K_{id}, is the slope of the line in stage 2 [182].

3.4.2.4 Liquid film diffusion model

According to the liquid film diffusion model, the longest phase of the adsorption process is the flow of adsorbate particles through a liquid film surrounding the solid adsorbent (i.e., the one that determines the kinetics of the velocity processes).

The liquid film diffusion model is shown in **Eq. 21.**

$$ln(1 - F) = K_{fd}t \qquad \textbf{Eq. 21}$$

Where;

F : The ratio (F = qt/qe) reached at the equilibrium.

K_{fd} : The film diffusion coefficient (min^{-1}).

When ln (1 – F) vs. t is plotted linearly, intercept is zero, the kinetics of the adsorption process are controlled by diffusion through the liquid film enclosing the cellulose-based polymers.

Table 3.17 (in appendix A) shows liquid film diffusion model values.

Table 3.18 (in appendix A) represents Adsorption kinetic parameters (Liquid film diffusion model) for the adsorption of Pb^{2+} on Cell-X-ZWC.

Figure 3.16 (in appendix B) shows the collected data for the Pb^{2+} adsorption by the Cell-X-ZWC polymers to the liquid film diffusion model.

The figure exhibited an extremely low correlation coefficient of 0.485 and no linear lines that crossed the origin. This shows that the step that influences the rate of adsorption is not the diffusion of adsorbate through the liquid film surrounding the Cell-X-ZWC based polymers.

It was discovered that the film diffusion coefficient was lower than the intraparticle coefficient, demonstrating that the diffusion to the external surface may be the rate-limiting stage in the adsorption mechanism.

For the whole adsorption process, the pseudo second-order kinetic model offers the best correlation, whereas the intraparticle diffusion model is only fit for the initial stages of the adsorption process. Consequently, it was concluded that the intraparticle diffusion was found to be rate limiting, followed by the pseudo second-order kinetic model [182].

3.4.3 Thermodynamics adsorption by Cell-X-ZWC polymer

The thermodynamic data of the adsorption of Pb^{2+} ions by Cell-X-ZWC polymer was also significant to evaluated, so these studies were performed at various temperatures.

Measurable thermodynamic parameters like temperature equilibrium constant, as well as their non-measurable equivalents like enthalpy ($\Delta H°$), entropy ($\Delta S°$), Gibbs free energy change ($\Delta G°$) and so on, are critical design factors. These parameters determine the spontaneity and feasibility of such processes.

Using the Van't Hoff plot's thermodynamic equation. The slope and y-intercept of the graph In (K_d) versus (1/T) can be used to calculate the thermodynamic parameters (ΔH° and ΔS°) of lead ions absorption on Cell-X-ZWC [184].

The parameters were calculated according to the following equations [40, 132, 185]:

$$K_C = \frac{C_{asd}}{C_e} \qquad \textbf{Eq .22}$$

Where;

Kc : is an apparent constant of the thermodynamics.

C_{ads} : is the amount adsorbed at equilibrium (mg/L).

C_e : is the equilibrium concentration in an aqueous solution of metal ion (mg/ L).

$$K_d = \frac{q_e}{C_e} \qquad \textbf{Eq .23}$$

Where;

K_d : the thermodynamic equilibrium constant (mol or L/g).

q_e : the equilibrium amount of solute adsorbed per unit weight of adsorbent.

$$\Delta G° = -RTlnk_d \qquad \textbf{Eq.24}$$

Where;

R : is the universal gas constant (J/mol K).

T : is the solution temperature (K).

$$lnk_d = \frac{\Delta S°}{R} - \frac{\Delta H°}{RT} \qquad \textbf{Eq.25}$$

So plotting lnK_d against (1/T) in the Van't Hoff plot will give a slope with a gradient of (-ΔH°/R) and an intercept of (ΔS°/R).

Table 3.19 (in appendix A) shows Thermodynamic value for Van't Hoff plots**.**

Table 3.20 (in appendix A) represents Pb^{2+} adsorption on polymer thermodynamic parameters.

Figure 3.17(in appendix B) represents Van't Hoff diagram showing Pb^{2+} adsorption on Cell-X-ZWC.

Since all of the ΔG° values in **Table 3.20** are negative, it is indicating that the lead ions adsorption on Cell-X-ZWC occurred spontaneously. A spontaneous process is one that takes place without the use of additional external energy. Also, the entropy (ΔH°<0), indicating an exothermic process and thus inexpensive reaction.

Finally, since (ΔS°<0), this suggests that the reaction occurs spontaneously at low temperatures, which is compatible with our result that the optimum adsorption occurs at 20°C. The adsorbent internal structure does not change significantly during the adsorption process, according to the negative value of ΔS°.

3.5 Real wastewater purification from metals

As we mentioned before (**sec. 2.5**) a real sample of sewage water was used in order to test the Cell-X-ZWC polymer efficiency in adsorbing of harmful heavy metal ions. **Table 3.21 (in appendix A**) shows the concentration of heavy metals before and after employing the polymers. ICP-MS was used to determine the concentration of metal ions.

The Cell-X-ZWC polymer shows a high efficiency for the harmful metal ions with high concentrations such as Ag^{+}, Al^{3+},Bi^{3+},Zn^{2+}, in addition to Pb^{2+}, Cu^{2+} with 97.77%, 90.39%, 93.03%, 88.88%, 85.17%, 87.54% respectively, and other ions.

Also, Cell-X-ZWC polymer Showed highly sensitivity to even low concentration of ions, such as Cd^{2+}, Te^{2+}, Be^{2+} with 90.85%, 81.85%, 95.68% respectively and other harmful ions.

3.6 Conclusion

In this work, cellulose with unique pendant groups composed of ammonium, amine and sulfonate, presence was prepared and used as an adsorbent for metal ions present in water. The presence of these groups on same repeat unit create zwitterion functionality as coordination sites for metal and anions with high degree of selectivity. The target cellulose based-zwitterionic was synthesized by oxidation of cellulose then crosslinking of cellulose by reacting it with 1,4-phenelendiamine then reacting with 1,4-butane sultone. The structure of the generated polymers was detected using FT-IR. Adsorption efficiency of Pb^{2+} by the prepared polymer was determined as function of temperature, time, initial concertation, adsorption dosage, and pH values have been found to provide the polymers with the greatest adsorption efficiency.

The developed Cell-X-ZWC exhibited excellent results in adsorbing heavy metals from wastewater, with the maximum adsorption result for lead being 97.43% at pH ≈7.21, polymer dose is about 20 mg, metal ion initial concertation 10 ppm with time 20 min of mixing at 20°C. The thermodynamic parameters of Pb^{2+} adsorption are spontaneous ($\Delta G°<0$), exothermic process ($\Delta H°<0$) and the reaction occurs spontaneously at low temperatures ($\Delta S°<0$). The adsorption process was following the pseudo second order kinetic adsorption model (R^2= 0.99) which was established by the adsorption parameters, and these adsorptions were matched with the Freundlich isotherm of adsorption (R^2=0.89).

3.7 Recommendations

1. The polymer can be given additional components to increase its efficiency for absorption.
2. In the water treatment process, this polymer can be examined for other toxic heavy metals.
3. This polymer can be studied for a variety of uses in the pharmaceutical field and drug administration.

List of Abbreviations

Abbreviations	Meaning
WHO	World Health Organization
TLVs	Threshold Limit Values
CNCs	Cellulose Nano Crystals
DMPC	1,2-dimyristoyl-sn-glycero-3-phosphatidylcholine
DMSP	3-dimethylsulfoniopropionate
Z	Atomic Number
DP	Degree Of Polymerization
OISW	Olive Industry Solid Waste
CMC	Carboxy Methyl Cellulose
NCC	Nanocrystalline Cellulose
DAC	Dialdehyde Cellulose
MNCs	Magnetic Cellulose Nanocrystalline
PPD	p-Phenylenediamine
PANI	Polyaniline
FT-IR	Fourier-Transform Infrared Spectrophotometer
FAAS	Flame Atomic Adsorption Spectrometer
ICP-MS	Inductively Coupled Plasma Mass Spectrometry
Cell-X	Crosslinked Cellulose
Cell-X-ZWC	Crosslinked Cellulose With Zwitterionic Functionality
R^2	Correlation coefficient (regression coefficient, fitting coefficient)
C_f	Concentration of metal ions at equilibrium in the sample solution after treatment (mg/L)
C_i	Initial concentration of metal ions in the sample solution (mg/L)
q_e	The mass of adsorbate adsorbed per unit mass of adsorbent at equilibrium (mg/g)
q_t	Amount of adsorbate per unit mass of adsorbent at time t (min)

K_1	The pseudo-first order rate constant
K_2	The pseudo-second order rate constant
K_f	Freundlich constant
K_L	Langmuir isotherm constant
K_d	The thermodynamic gas constant
1/n	Dimensionless Freundlich constant
R_L	Separation factor dimensionless constant
Δ H°	The change in enthalpy
Δ S°	The change in entropy
Δ G°	The change in Gibbs free energy
R	The universal gas constant
T	The Absolut temperature
DS	Degree of substitutions
K_{id}	The Intraparticle Diffusion Rate Constant
Z	The Thickness Of The Boundary Layer
K_{fd}	The Film Diffusion Coefficient

References

1. Kılıç, Z.J.I.J.o.H., *The importance of water and conscious use of water.* 2020. **4**(5): p. 239-241.

2. Ahmed, S., et al., *Water pollution and its sources, effects & management: a case study of Delhi.* 2018. **7**(2): p. 10436-10442.

3. Voulvoulis, N.J.C.O.i.E.S. and Health, *Water reuse from a circular economy perspective and potential risks from an unregulated approach.* 2018. **2**: p. 32-45.

4. Yuan, M.-H. and S.-L.J.E.S. Lo, *Ecosystem services and sustainable development: Perspectives from the food-energy-water Nexus.* 2020. **46**: p. 101217.

5. He, M., et al., *Waste-derived biochar for water pollution control and sustainable development.* 2022. **3**(7): p. 444-460.

6. Wang, Q., et al., *Sustainable cellulose nanomaterials for environmental remediation-achieving clean air, water, and energy: a review.* 2022: p. 119251.

7. Zamora-Ledezma, C., et al., *Heavy metal water pollution: A fresh look about hazards, novel and conventional remediation methods.* 2021. **22**: p. 101504.

8. Liu, Y., et al., *A review of water pollution arising from agriculture and mining activities in Central Asia: Facts, causes and effects.* 2021. **291**: p. 118209.

9. Haseena, M., et al., *Water pollution and human health.* 2017. **1**(3).

10. Hojjati-Najafabadi, A., et al., *A review on magnetic sensors for monitoring of hazardous pollutants in water resources.* 2022. **824**: p. 153844.

11. Ogidi, O.I. and U.M. Akpan, *Aquatic Biodiversity Loss: Impacts of Pollution and Anthropogenic Activities and Strategies for Conservation*, in *Biodiversity in Africa: Potentials, Threats and Conservation*. 2022, Springer. p. 421-448.

12. Takarina, N.D., A.I.S. Purwiyanto, and Y.J.M.P.B. Suteja, *Cadmium (Cd), Copper (Cu), and Zinc (Zn) levels in commercial and non-commercial fishes in*

the Blanakan River Estuary, Indonesia: A preliminary study. 2021. **170**: p. 112607.

13. Masindi, V. and K.L.J.H.m. Muedi, *Environmental contamination by heavy metals.* 2018. **10**: p. 115-132.

14. Hasani, N., et al., *Theoretical, Equilibrium, Kinetics and Thermodynamic Investigations of Methylene Blue Adsorption onto Lignite Coal.* 2022. **27**(6): p. 1856.

15. Rahman, Z., V.P.J.E.m. Singh, and assessment, *The relative impact of toxic heavy metals (THMs)(arsenic (As), cadmium (Cd), chromium (Cr)(VI), mercury (Hg), and lead (Pb)) on the total environment: an overview.* 2019. **191**(7): p. 1-21.

16. Balali-Mood, M., et al., *Toxic mechanisms of five heavy metals: mercury, lead, chromium, cadmium, and arsenic.* 2021. **12**: p. 643972.

17. Topare, N.S. and V.S.J.M.T.P. Wadgaonkar, *A review on application of low-cost adsorbents for heavy metals removal from wastewater.* 2022.

18. Varsha, M., P.S. Kumar, and B.S.J.C. Rathi, *A review on recent trends in the removal of emerging contaminants from aquatic environment using low-cost adsorbents.* 2022. **287**: p. 132270.

19. Ge, H. and J.J.C. Wang, *Ear-like poly (acrylic acid)-activated carbon nanocomposite: A highly efficient adsorbent for removal of Cd (II) from aqueous solutions.* 2017. **169**: p. 443-449.

20. Sezgin, N., N.J.D. Balkaya, and W. Treatment, *Adsorption of heavy metals from industrial wastewater by using polyacrylic acid hydrogel.* 2016. **57**(6): p. 2466-2480.

21. Gafur, N.A., et al., *A case study of heavy metal pollution in water of Bone River by Artisanal Small-Scale Gold Mine Activities in Eastern Part of Gorontalo, Indonesia.* 2018. **10**(11): p. 1507.

22. Okereafor, U., et al., *Toxic metal implications on agricultural soils, plants, animals, aquatic life and human health.* 2020. **17**(7): p. 2204.

23. Joseph, L., et al., *Removal of heavy metals from water sources in the developing world using low-cost materials: A review.* 2019. **229**: p. 142-159.

24. Herath, I.K., et al., *Heavy metal toxicity, ecological risk assessment, and pollution sources in a hydropower reservoir.* 2022. **29**(22): p. 32929-32946.

25. Brescia, S.J.C.R.i.T., *Thresholds of adversity and their applicability to endocrine disrupting chemicals.* 2020. **50**(3): p. 213-218.

26. Lawal, K.K., et al., *A review on the public health implications of heavy metals.* 2021. **10**(3): p. 255-265.

27. Burnase, N., S. Jaiswal, and A. Barapatre, *Metal Toxicity in Humans Associated with Their Occupational Exposures Due to Mining*, in *Medical Geology in Mining*. 2022, Springer. p. 127-186.

28. Jamjoum, H.A., S. Kamaruzaman, and N.A.J.A.o.t.R.S.f.C.B. Yusof, *ADSORPTIVE STUDY OF COPPER (CU2+) IN AQUEOUS SAMPLES USING EFFERVESCENCE AMINO-ZEOLITE.* 2021: p. 13067-13079.

29. Borobia, M., et al., *Copper Poisoning, a Deadly Hazard for Sheep.* 2022. **12**(18): p. 2388.

30. Dasharathy, S., et al., *Mutagenic, Carcinogenic, and Teratogenic Effect of Heavy Metals.* 2022. **2022**.

31. Ilesanmi, O.B. and E.R.J.T.A.e.C. Inala, *Hepatoprotective effect of Ipomoea cairica (Convolvulaceae) leaf extract against cadmium chloride induced liver damage.* 2022. **34**(1): p. 30-37.

32. Jaishankar, M., et al., *Toxicity, mechanism and health effects of some heavy metals.* 2014. **7**(2): p. 60.

33. Ventre, S., et al., *Toxic metal exposures from infant diets: Risk prevention strategies for caregivers and health care professionals.* 2022: p. 101276.

34. Baby Shaikh, R., B. Saifullah, and F.U.J.W. Rehman, *Greener method for the removal of toxic metal ions from the wastewater by application of agricultural waste as an adsorbent.* 2018. **10**(10): p. 1316.

35. Wang, H., et al., *Water and wastewater treatment in Africa–current practices and challenges.* 2014. **42**(8): p. 1029-1035.

36. Saleh, T.A.J.E.T. and Innovation, *Protocols for synthesis of nanomaterials, polymers, and green materials as adsorbents for water treatment technologies.* 2021. **24**: p. 101821.

37. Fatta-Kassinos, D., D.D. Dionysiou, and K. Kümmerer, *Advanced treatment technologies for urban wastewater reuse*. 2016: Springer.

38. Kavitha, C., et al., *Elimination of Lead by Biosorption on Parthenium stem powder using Box-Behnken Design.* 2022. **42**: p. 270-279.

39. Tamjidi, S., A.J.E.S. Ameri, and P. Research, *A review of the application of sea material shells as low cost and effective bio-adsorbent for removal of heavy metals from wastewater*. 2020. **27**(25): p. 31105-31119.

40. Wang, L., et al., *Rational design, synthesis, adsorption principles and applications of metal oxide adsorbents: a review*. 2020. **12**(8): p. 4790-4815.

41. Mandal, S., et al., *Mesoporous activated carbon as a green adsorbent for the removal of heavy metals and Congo red: Characterization, adsorption kinetics, and isotherm studies.* 2021. **243**: p. 103869.

42. Gu, S., et al., *Clay mineral adsorbents for heavy metal removal from wastewater: a review*. 2019. **17**(2): p. 629-654.

43. Erman, I., *Zeolite/Cellulose Acetate (ZCA) in Blend Fiber for Removal of Erythromycin from Aqueous Solution Experimental and Theoretical Study*. 2021, جامعة النجاح الوطنية.

44. Lin, J., et al., *Durably antibacterial and bacterially antiadhesive cotton fabrics coated by cationic fluorinated polymers.* 2018. **10**(7): p. 6124-6136.

45. Keller, V., et al., *Effectiveness of fly ash and red mud as strategies for sustainable acid mine drainage management.* 2020. **10**(8): p. 707.

46. Jodeh, S., et al., *Magnetic nanocellulose from olive industry solid waste for the effective removal of methylene blue from wastewater*. 2018. **25**(22): p. 22060-22074.

47. Mo, J., et al., *A review on agro-industrial waste (AIW) derived adsorbents for water and wastewater treatment.* 2018. **227**: p. 395-405.

48. Razak, M.R., et al., *Iminodiacetic acid modified kenaf fiber for waste water treatment.* 2018. **112**: p. 754-760.

49. Du, J., et al., *Radiation grafting of dimethylaminoethyl methacrylate on cotton linter and subsequent quaternization as new eco-friendly adsorbent for phosphate removal.* 2020. **27**(19): p. 24558-24567.

50. Sipponen, M.H. and M.J.F.i.C. Österberg, *Aqueous Ammonia pre-treatment of wheat straw: Process optimization and broad spectrum dye adsorption on nitrogen-containing lignin.* 2019. **7**: p. 545.

51. Chikri, R., N. Elhadiri, and M.J.J.o.C. Benchanaa, *Efficiency of sawdust as low-cost adsorbent for dyes removal.* 2020. **2020**.

52. Zhan, C., et al., *Rice husk based nanocellulose scaffolds for highly efficient removal of heavy metal ions from contaminated water.* 2020. **6**(11): p. 3080-3090.

53. Chakraborty, R., et al., *Adsorption of heavy metal ions by various low-cost adsorbents: a review*. 2022. **102**(2): p. 342-379.

54. Wang, J., et al., *Preparation and characterization of cellulose-based adsorbent and its application in heavy metal ions removal.* 2019. **206**: p. 837-843.

55. Mitchell, D.E., N.R. Cameron, and M.I.J.C.C. Gibson, *Rational, yet simple, design and synthesis of an antifreeze-protein inspired polymer for cellular cryopreservation.* 2015. **51**(65): p. 12977-12980.

56. Ihsan, A.B., et al., *Self-healing behaviors of tough polyampholyte hydrogels.* 2016. **49**(11): p. 4245-4252.

57. La, T.-G., et al., *Highly flexible, multipixelated thermosensitive smart windows made of tough hydrogels.* 2017. **9**(38): p. 33100-33106.

58. Gao, X., et al., *Removal of heavy metal and sulfate ions by cellulose derivative-based biosorbents.* 2018. **25**(4): p. 2531-2545.

59. Liu, C., et al., *Adsorption behavior of carboxylated cellulose nanocrystal—polyethyleneimine composite for removal of Cr (VI) ions.* 2017. **408**: p. 77-87.

60. Zhou, H., et al., *Cellulose-based amphoteric adsorbent for the complete removal of low-level heavy metal ions via a specialization and cooperation mechanism.* 2020. **385**: p. 123879.

61. Geng, X., G. Shi, and G.J.J.o.A.P.S. Wu, *Damping properties of acrylate polymers mediated by ionic coordination.* 2022. **139**(40): p. e52969.

62. Blackman, L.D., et al., *An introduction to zwitterionic polymer behavior and applications in solution and at surfaces.* 2019. **48**(3): p. 757-770.

63. Mishra, M., *Encyclopedia of Polymer Applications, 3 Volume Set*. 2018: CRC press.

64. Lowe, A.B. and C.L.J.C.r. McCormick, *Synthesis and solution properties of zwitterionic polymers.* 2002. **102**(11): p. 4177-4190.

65. Lamb, J.R., C.M. Brown, and J.A.J.C.S. Johnson, *N-Heterocyclic carbene–carbodiimide (NHC–CDI) betaine adducts: synthesis, characterization, properties, and applications.* 2021. **12**(8): p. 2699-2715.

66. Zurick, K.M. and M.J.J.o.A.P.S. Bernards, *Recent biomedical advances with polyampholyte polymers.* 2014. **131**(6).

67. Erkoc, P. and F.J.P. Ulucan-Karnak, *Nanotechnology-based antimicrobial and antiviral surface coating strategies.* 2021. **3**(1): p. 25-52.

68. Mangal, U., J.-S. Kwon, and S.-H.J.I.J.o.M.S. Choi, *Bio-interactive zwitterionic dental biomaterials for improving biofilm resistance: Characteristics and applications.* 2020. **21**(23): p. 9087.

69. Brown, R.H., et al., *Effect of ionic liquid on mechanical properties and morphology of zwitterionic copolymer membranes.* 2010. **43**(2): p. 790-796.

70. Wu, T., et al., *Influence of zwitterions on thermomechanical properties and morphology of acrylic copolymers: implications for electroactive applications.* 2011. **44**(20): p. 8056-8063.

71. Laschewsky, A.J.P., *Structures and synthesis of zwitterionic polymers.* 2014. **6**(5): p. 1544-1601.

72. Van Tran, T.T., S.R. Kumar, and S.J.J.J.o.M.S. Lue, *Separation mechanisms of binary dye mixtures using a PVDF ultrafiltration membrane: Donnan effect and intermolecular interaction.* 2019. **575**: p. 38-49.

73. Krebs, I., *Zwitterion-Perylene diimide-Modules for switchable supramolecular systems*. 2016, Duisburg, Essen, Universität Duisburg-Essen, Diss., 2015.

74. Obiweluozor, F.O., et al., *A NIPAM–zwitterion copolymer: rheological interpretation of the specific ion effect on the LCST.* 2014. **215**(11): p. 1077-1091.

75. Li, S., et al., *Comb-shaped polyzwitterion with surface-activity obtained via N-maleoyl chitosan-modified HPAM for displacement of residual oil.* 2018. **42**(9): p. 6848-6857.

76. Biehl, P., et al., *Synthesis, characterization, and applications of magnetic nanoparticles featuring polyzwitterionic coatings.* 2018. **10**(1): p. 91.

77. Moriwaki, S., Y. Yoshizaki, and T.J.J.o.M.C.B. Konno, *Phospholipid polymer hydrogels with rapid dissociation for reversible cell immobilization.* 2022. **10**(14): p. 2628-2636.

78. Jiang, S. and Z.J.A.m. Cao, *Ultralow-fouling, functionalizable, and hydrolyzable zwitterionic materials and their derivatives for biological applications.* 2010. **22**(9): p. 920-932.

79. Grainger, D.W.J.N.b., *All charged up about implanted biomaterials.* 2013. **31**(6): p. 507-509.

80. He, M., et al., *Zwitterionic materials for antifouling membrane surface construction.* 2016. **40**: p. 142-152.

81. Liu, J., et al., *Preparation of zwitterionic hybrid polymer and its application for the removal of heavy metal ions from water.* 2010. **178**(1-3): p. 1021-1029.

82. Venault, A., et al., *Surface self-assembled zwitterionization of poly (vinylidene fluoride) microfiltration membranes via hydrophobic-driven coating for improved blood compatibility.* 2014. **454**: p. 253-263.

83. Zhou, T., et al., *Removal of Pb (II) from aqueous solutions using waste textiles/poly (acrylic acid) composite synthesized by radical polymerization technique.* 2018. **67**: p. 368-377.

84. Dotto, G.L. and G.J.J.o.e.c.e. McKay, *Current scenario and challenges in adsorption for water treatment.* 2020. **8**(4): p. 103988.

85. Maksoud, M.A., et al., *Insight on water remediation application using magnetic nanomaterials and biosorbents.* 2020. **403**: p. 213096.

86. Saleh, T.A., *Adsorption technology and surface science*, in *Interface Science and Technology*. 2022, Elsevier. p. 39-64.

87. Dąbrowski, A.J.A.i.c. and i. science, *Adsorption—from theory to practice.* 2001. **93**(1-3): p. 135-224.

88. Brandenburg, J.G., et al., *Physisorption of water on graphene: Subchemical accuracy from many-body electronic structure methods.* 2019. **10**(3): p. 358-368.

89. Schlumberger, C. and M.J.A.M.I. Thommes, *Characterization of hierarchically ordered porous materials by physisorption and mercury porosimetry—A tutorial review.* 2021. **8**(4): p. 2002181.

90. Králik, M.J.C.P., *Adsorption, chemisorption, and catalysis.* 2014. **68**(12): p. 1625-1638.

91. Khalaf, B.M.M., *Purification of Groundwater from Heavy Toxic Metals using Suspended Polydentate Supported Ligands*. 2016.

92. Pourret, O., J.-C. Bollinger, and A.J.A.G. Hursthouse, *Heavy metal: a misused term?* 2021. **40**(3): p. 466-471.

93. Ali, H., E.J.T. Khan, and E. Chemistry, *What are heavy metals? Long-standing controversy over the scientific use of the term 'heavy metals'–proposal of a comprehensive definition.* 2018. **100**(1): p. 6-19.

94. Rangabhashiyam, S. and P.J.B.t.r. Balasubramanian, *Characteristics, performances, equilibrium and kinetic modeling aspects of heavy metal removal using algae.* 2019. **5**: p. 261-279.

95. Mohammed, A.S., A. Kapri, and R. Goel, *Heavy metal pollution: source, impact, and remedies*, in *Biomanagement of metal-contaminated soils*. 2011, Springer. p. 1-28.

96. Sardar, K., et al., *Heavy metals contamination and what are the impacts on living organisms.* 2013. **2**(4): p. 172-179.

97. Febrianto, J., et al., *Equilibrium and kinetic studies in adsorption of heavy metals using biosorbent: a summary of recent studies.* 2009. **162**(2-3): p. 616-645.

98. Larous, S., A.-H. Meniai, and M.B.J.D. Lehocine, *Experimental study of the removal of copper from aqueous solutions by adsorption using sawdust.* 2005. **185**(1-3): p. 483-490.

99. Ganesan, S., *Waste Fruit Cortexes for the Removal of Heavy Metals from Water*, in *Green Adsorbents to Remove Metals, Dyes and Boron from Polluted Water*. 2021, Springer. p. 323-350.

100. Alghamdi, A.A., et al., *Efficient adsorption of lead (II) from aqueous phase solutions using polypyrrole-based activated carbon.* 2019. **12**(12): p. 2020.

101. Maraz, K.M., et al., *Development of Biodegradable Packaging Materials from Bio-Based Raw Materials.* 2019. **8**: p. 66-84.

102. Eyley, S. and W.J.N. Thielemans, *Surface modification of cellulose nanocrystals.* 2014. **6**(14): p. 7764-7779.

103. Ahamed, M.I., E. Lichtfouse, and A.M. Asiri, *Green Adsorbents to Remove Metals, Dyes and Boron from Polluted Water*. 2021: Springer.

104. Baghaei, B. and M.J.M. Skrifvars, *All-cellulose composites: A review of recent studies on structure, properties and applications.* 2020. **25**(12): p. 2836.

105. دهماز، ا., *CELLULOSE GRAFTED WITH β-CYCLODEXTRIN FOR WASTE WATER PURIFICATION FROM TOXIC METAL IONS*. 2019, جامعة النجاح الوطنية.

106. Thomas, P., et al., *Comprehensive review on nanocellulose: Recent developments, challenges and future prospects.* 2020. **110**: p. 103884.

107. Blanco, A., et al., *Nanocellulose for industrial use: cellulose nanofibers (CNF), cellulose nanocrystals (CNC), and bacterial cellulose (BC)*, in *Handbook of nanomaterials for industrial applications*. 2018, Elsevier. p. 74-126.

108. Peng, B.L., et al., *Chemistry and applications of nanocrystalline cellulose and its derivatives: a nanotechnology perspective.* 2011. **89**(5): p. 1191-1206.

109. Long, L.-Y., Y.-X. Weng, and Y.-Z.J.P. Wang, *Cellulose aerogels: Synthesis, applications, and prospects.* 2018. **10**(6): p. 623.

110. Czarnecka, E. and J.J.I.j.o.m.s. Nowaczyk, *Synthesis and characterization superabsorbent polymers made of starch, acrylic acid, acrylamide, poly (Vinyl*

alcohol), 2-hydroxyethyl methacrylate, 2-acrylamido-2-methylpropane sulfonic acid. 2021. **22**(9): p. 4325.

111. Hamed, O.A., et al., *Cellulose Powder Functionalized with Phenyl Biguanide: Synthesis, Cross-Linking, Metal Adsorption, and Molecular Docking*. 2021. **16**(4): p. 7263-7282.

112. Nairat, N., et al., *Cellulose polymers with β-amino ester pendant group: design, synthesis, molecular docking and application in adsorption of toxic metals from wastewater*. 2022. **16**(1): p. 1-21.

113. غ ،شقدان. and ابتهال, *Anionic Microcrystalline Cellulose For Removal of Pb+ 2 From Waste Water Purification*. 2020, جامعة النجاح الوطنية.

114. Hamed, O., et al., *Synthesis of a cross-linked cellulose-based amine polymer and its application in wastewater purification*. 2019. **26**: p. 28080-28091.

115. Deghles, A., et al., *Cellulose with bidentate chelating functionality: an adsorbent for metal ions from wastewater*. 2019. **14**(3): p. 6247-6266.

116. ر ،"خليف. and احمد .ب.ق, *Synthesis of Three Dimensional Cellulose Diamine Polymer for Wastewater Purification*. 2018, An-Najah National University.

117. saad Algarni, T. and A.M.J.J.o.K.S.U.-S. Al-Mohaimeed, *Water purification by absorption of pigments or pollutants via metaloxide*. 2022: p. 102339.

118. Baskar, A.V., et al., *Recovery, regeneration and sustainable management of spent adsorbents from wastewater treatment streams: A review*. 2022: p. 153555.

119. Gupta, V., et al., *Cellulose: a review as natural, modified and activated carbon adsorbent*. 2016. **216**: p. 1066-1076.

120. Loto, R. and C.J.I.J.o.E.S. Loto, *Effect of P-phenylediamine on the corrosion of austenitic stainless steel type 304 in hydrochloric acid*. 2012. **7**(10): p. 9423-9440.

121. Elmanfe, G.M., et al., *Determination of Para-Phenylenediamine (PPD) in Henna Samples Collected from Libyan Local Markets Using HPLC.* 2022. **37**(1): p. 13-21.

122. Mdlalose, L., et al., *The chemistry of Cr (VI) adsorption on to poly (p-phenylenediamine) adsorbent.* 2018. **78**(12): p. 2481-2488.

123. Chong, H., et al., *Para-phenylenediamine containing hair dye: An overview of mutagenicity, carcinogenicity and toxicity.* 2016. **6**(5): p. 1000403.

124. Kim, U.-J., et al., *Periodate oxidation of crystalline cellulose.* Biomacromolecules, 2000. **1**(3): p. 488-492.

125. Chowdhury, T., et al., *Pb (ii) adsorption from aqueous solution by an aluminum-based metal organic framework–graphene oxide nanocomposite.* Materials Advances, 2021. **2**(9): p. 3051-3059.

126. Zahoor, M., *Removal of pesticides from water using granular activated carbon and ultrafiltration membrane—a pilot plant study.* Journal of Encapsulation and adsorption sciences, 2013. **2013**.

127. Li, W., et al., *Enhanced adsorption capacity of ultralong hydrogen titanate nanobelts for antibiotics.* Journal of Materials Chemistry A, 2017. **5**(9): p. 4352-4358.

128. Zhou, Y., et al., *Heavy metal ions and organic dyes removal from water by cellulose modified with maleic anhydride.* Journal of Materials Science, 2012. **47**(12): p. 5019-5029.

129. Moyo, M., et al., *Adsorption batch studies on the removal of Pb (II) using maize tassel based activated carbon.* Journal of Chemistry, 2013. **2013**.

130. Hamed, O.A., et al., *Cellulose Powder Functionalized with Phenyl Biguanide: Synthesis, Cross-Linking, Metal Adsorption, and Molecular Docking.* BioResources, 2021. **16**(4): p. 7263-7282.

131. Sud, D., G. Mahajan, and M. Kaur, *Agricultural waste material as potential adsorbent for sequestering heavy metal ions from aqueous solutions–A review.* Bioresource technology, 2008. **99**(14): p. 6017-6027.

132. Hamed, O., et al., *Synthesis of a cross-linked cellulose-based amine polymer and its application in wastewater purification.* 2019. **26**(27): p. 28080-28091.

133. Milonjić, S.K., *A consideration of the correct calculation of thermodynamic parameters of adsorption.* Journal of the Serbian chemical society, 2007. **72**(12): p. 1363-1367.

134. Potgieter, J., S. Pearson, and C. Pardesi, *Kinetic and thermodynamic parameters for the adsorption of methylene blue using fly ash under batch, column, and heap leaching configurations.* Coal combustion and gasification products, 2018. **10**(2): p. 23-33.

135. Hamed, O., et al., *Synthesis of a cross-linked cellulose-based amine polymer and its application in wastewater purification.* Environmental Science and Pollution Research, 2019. **26**(27): p. 28080-28091.

136. Raghav, S. and D. Kumar, *Adsorption equilibrium, kinetics, and thermodynamic studies of fluoride adsorbed by tetrametallic oxide adsorbent.* Journal of Chemical & Engineering data, 2018. **63**(5): p. 1682-1697.

137. Revellame, E.D., et al., *Adsorption kinetic modeling using pseudo-first order and pseudo-second order rate laws: A review.* Cleaner Engineering and Technology, 2020. **1**: p. 100032.

138. de Cuadro, P., et al., *Cross-linking of cellulose and poly (ethylene glycol) with citric acid.* Reactive and Functional Polymers, 2015. **90**: p. 21-24.

139. Bin-Dahman, O.A., J. Jose, and M.A. Al-Harthi, *Compatibility of poly (acrylic acid)/starch blends.* Starch-Stärke, 2015. **67**(11-12): p. 1061-1069.

140. Anirudhan, T. and P. Radhakrishnan, *Thermodynamics and kinetics of adsorption of Cu (II) from aqueous solutions onto a new cation exchanger*

derived from tamarind fruit shell. The Journal of Chemical Thermodynamics, 2008. **40**(4): p. 702-709.

141. Jackson, E.L. and C. Hudson, *Application of the cleavage type of oxidation by periodic acid to starch and cellulose1*. Journal of the American Chemical Society, 1937. **59**(10): p. 2049-2050.

142. Jackson, E.L. and C. Hudson, *The Structure of the Products of the Periodic Acid Oxidation of Starch and Cellulose1*. Journal of the American chemical society, 1938. **60**(5): p. 989-991.

143. Morooka, T., M. Norimoto, and T. Yamada, *Periodate oxidation of cellulose by homogeneous reaction.* Journal of applied polymer science, 1989. **38**(5): p. 849-858.

144. Höglund, E. *Production of Dialdehyde Cellulose and Periodate Regeneration: Towards feasible oxidation processes*. 2015.

145. Sahin, H.T.J.A.S.S., *RF-CF4 plasma surface modification of paper: Chemical evaluation of two sidedness with XPS/ATR-FTIR.* 2007. **253**(9): p. 4367-4373.

146. Daoud, W.A., et al., *Pulsed laser deposition of superhydrophobic thin Teflon films on cellulosic fibers.* 2006. **515**(2): p. 835-837.

147. Cleary, J.A., et al., *Hemiacetal stabilization in a chymotrypsin inhibitor complex and the reactivity of the hydroxyl group of the catalytic serine residue of chymotrypsin.* 2014. **1844**(6): p. 1119-1127.

148. Bayer, I.S., et al., *Superhydrophobic cellulose-based bionanocomposite films from Pickering emulsions.* 2009. **94**(16): p. 163902.

149. Passiniemi, M. and A.M.J.B.J.o.O.C. Koskinen, *Garner's aldehyde as a versatile intermediate in the synthesis of enantiopure natural products.* 2013. **9**(1): p. 2641-2659.

150. Tan, W.-Y., et al., *Oxidation of Primary Alcohols and Aldehydes to Carboxylic Acids via Hydrogen Atom Transfer*. 2021. **23**(17): p. 6648-6653.

151. Hofreiter, B., I. Wolff, and C.J.J.o.t.A.C.S. Mehltretter, *Chlorous Acid Oxidation of Periodate Oxidized Cornstarch2.* 1957. **79**(24): p. 6457-6460.

152. Casu, B., et al., *Stereoregular acyclic polyalcohols and polyacetates from cellulose and amylose.* 1985. **18**(12): p. 2762-2767.

153. Maekawa, E. and T.J.J.o.A.P.S. Koshijima, *Preparation and structural consideration of nitrogen-containing derivatives obtained from dialdehyde celluloses.* 1991. **42**(1): p. 169-178.

154. Appel, R. and H.J.J.o.t.A.C.S. Mayr, *Quantification of the electrophilic reactivities of aldehydes, imines, and enones.* 2011. **133**(21): p. 8240-8251.

155. Hashimoto, S., T. Yamashita, and M.J.P.J. Kaneda, *The Ring-Opening Polymerization of Sultones. VII. Thermodynamic Parameters of 3-Hydroxy-1-propane Sulfonic Acid Sultone for Ring-Opening Polymerization.* 1974. **6**(3): p. 238-241.

156. Hess, M., et al., *Terminology of polymers containing ionizable or ionic groups and of polymers containing ions (IUPAC Recommendations 2006).* 2006. **78**(11): p. 2067-2074.

157. Lo, S.-F., et al., *Adsorption capacity and removal efficiency of heavy metal ions by Moso and Ma bamboo activated carbons.* 2012. **90**(9): p. 1397-1406.

158. Zhang, Y., et al., *Adsorption equilibrium and kinetics of the removal of ammoniacal nitrogen by zeolite X/activated carbon composite synthesized from elutrilithe.* 2017. **2017**.

159. Chen, K., et al., *Removal of cadmium and lead ions from water by sulfonated magnetic nanoparticle adsorbents.* 2017. **494**: p. 307-316.

160. Akbar, N.A., H.A. Aziz, and M.N.J.J.T. Adlan, *Potential of high quality limestone as adsorbent for iron and manganese removal in groundwater.* 2016. **78**(9-4).

161. Zhang, B., et al., *Adsorption of copper (II) and lead (II) ions onto cottonseed protein-PAA hydrogel composite.* 2012. **51**(6): p. 612-619.

162. Kajjumba, G.W., et al., *Modelling of adsorption kinetic processes—errors, theory and application.* 2018: p. 1-19.

163. Rao, M.M., et al., *Activated carbon from Ceiba pentandra hulls, an agricultural waste, as an adsorbent in the removal of lead and zinc from aqueous solutions.* 2008. **28**(5): p. 849-858.

164. Boparai, H.K., M. Joseph, and D.M.J.J.o.h.m. O'Carroll, *Kinetics and thermodynamics of cadmium ion removal by adsorption onto nano zerovalent iron particles.* 2011. **186**(1): p. 458-465.

165. Azmi, A., et al., *The influence of temperature on adsorption capacity of Malaysian coal.* 2006. **45**(5): p. 392-396.

166. Liu, L., et al., *Application of nanotechnology in the removal of heavy metal from water*, in *Nanomaterials for the removal of pollutants and resource reutilization*. 2019, Elsevier. p. 83-147.

167. Marczewski, A.W., et al., *Adsorption equilibrium and kinetics of selected phenoxyacid pesticides on activated carbon: effect of temperature.* 2016. **22**(4): p. 777-790.

168. Weißpflog, J., et al., *Solubility and selectivity effects of the anion on the adsorption of different heavy metal ions onto chitosan.* 2020. **25**(11): p. 2482.

169. Mészáros, R., I. Varga, and T.J.L. Gilányi, *Adsorption of poly (ethyleneimine) on silica surfaces: effect of pH on the reversibility of adsorption.* 2004. **20**(12): p. 5026-5029.

170. Anirudhan, T. and S.J.J.o.E.S. Sreekumari, *Adsorptive removal of heavy metal ions from industrial effluents using activated carbon derived from waste coconut buttons.* 2011. **23**(12): p. 1989-1998.

171. Ebrahimi, F., et al., *Fabrication of nanofibers using sodium alginate and Poly (Vinyl alcohol) for the removal of Cd2+ ions from aqueous solutions: Adsorption mechanism, kinetics and thermodynamics.* 2019. **5**(11): p. e02941.

172. Crini, G., et al., *Removal of CI Basic Green 4 (Malachite Green) from aqueous solutions by adsorption using cyclodextrin-based adsorbent: kinetic and equilibrium studies.* 2007. **53**(1): p. 97-110.

173. Tiwari, A.N., et al., *A sustainable approach to Gilloy-shoot extract-mediated synthesis of magnetite nanoparticles: isotherm and kinetic study of U (VI) removal.* 2022. **331**(9): p. 3819-3833.

174. Kannan, N., M.J.W. Meenakshisundaram, air,, and s. pollution, *Adsorption of Congo Red on various activated carbons. A comparative study.* 2002. **138**(1): p. 289-305.

175. Meroufel, B., et al., *Adsorptive removal of anionic dye from aqueous solutions by Algerian kaolin: Characteristics, isotherm, kinetic and thermodynamic studies.* 2013. **4**(3): p. 482-491.

176. Cozmuta, L.M., et al., *The influence of pH on the adsorption of lead by Na-clinoptilolite: Kinetic and equilibrium studies.* 2012. **38**(2): p. 269-278.

177. Ofomaja, A.E., Y.-S.J.D. Ho, and Pigments, *Equilibrium sorption of anionic dye from aqueous solution by palm kernel fibre as sorbent.* 2007. **74**(1): p. 60-66.

178. Uddin, M.K.J.C.E.J., *A review on the adsorption of heavy metals by clay minerals, with special focus on the past decade.* 2017. **308**: p. 438-462.

179. Zhao, X., et al., *Synthesis and characterization of gadolinium doped cobalt ferrite nanoparticles with enhanced adsorption capability for Congo Red.* 2014. **250**: p. 164-174.

180. Khudariah, D.A.A., *Modification and Characterization of Novel Porous SiO2 Material Functionalized with C, C-Pyridylpyrazole acceptor for sulphate Removal from wastewater*. 2016.

181. Ofomaja, A.E., E.B. Naidoo, and A.J.S.A.J.o.C.E. Pholosi, *Intraparticle diffusion of Cr (VI) through biomass and magnetite coated biomass: A comparative kinetic and diffusion study*. 2020. **32**(1): p. 39-55.

182. Kumar, P.S. and R.J.J.E.S.T. Gayathri, *Adsorption of Pb2+ ions from aqueous solutions onto bael tree leaf powder: isotherms, kinetics and thermodynamics study*. 2009. **4**(4): p. 381-399.

183. Guo, X., S. Zhang, and X.-q.J.J.o.h.m. Shan, *Adsorption of metal ions on lignin.* 2008. **151**(1): p. 134-142.

184. Zhang, Z., et al., *Immobilization of lead and cadmium from aqueous solution and contaminated sediment using nano-hydroxyapatite*. 2010. **158**(2): p. 514-519.

185. Azzaoui, K., et al., *Novel tricomponenets composites films from polylactic Acid/Hydroxyapatite/Poly-Caprolactone suitable for Biomedical Applications.* 2016. **7**: p. 761-769.

Appendices

Appendix A

Tables

Table 3.11

Values of the pseudo-first order model.

Time (min)	$[Pb^{2+}]$ (ppm) C_e	q_t (mg/g)	$\ln(q_e-q_t)$
5	3.07	3.46	0.08
10	1.44	4.28	-1.32
15	1.53	4.23	-1.17
20	1.34	4.33	-1.53
25	1.78	4.11	-0.83
30	1.62	4.19	-1.03

Table 3.12

Adsorption kinetic parameters for the adsorption of Pb^{2+} on Cell-X-ZWC (pseudo-first order model).

Metal ion	R^2	Theo. q_e	Exp. q_e	K_1
Pb^{2+}	0.18	0.59	4.55	0.03

Table 3.13

Pseudo-second order model values

Time (min)	$[Pb^{2+}]$ (ppm) C_e	q_t (mg/g)	t/q_t
5	3.07	3.46	1.44
10	1.44	4.28	2.34
15	1.53	4.23	3.54
20	1.34	4.33	4.62
25	1.78	4.11	6.08
30	1.62	4.19	7.16

Table 3.14

Adsorption kinetic parameters for the adsorption of Pb^{2+} on Cell-X-ZWC (pseudo-second order model)

Metal ion	R^2	Theo. q_e	Exp. q_e	K_2
Pb^{2+}	0.99	4.28	4.55	0.51

Table 3.15

Intraparticle diffusion model values

Time (min)	$[Pb^{2+}]$ (ppm) C_e	q_t (mg/g)	$t^{1/2}$
5	3.07	3.46	2.24
10	1.44	4.28	3.16
15	1.53	4.23	3.87
20	1.34	4.33	4.47
25	1.78	4.11	5.00
30	1.62	4.19	5.48

Table 3.16

Kinetic adsorption parameters (Intraparticle diffusion model) for the adsorption of Pb^{2+} on Cell-X-ZWC.

Metal ion	R^2	Z	K_{id}
Pb^{2+}	0.75	1.00	0.73

Table 3.17

liquid film diffusion model values

Time (min)	$[Pb^{2+}]$ (ppm) C_e	q_t (mg/g)	ln(1- F) q_e = 4.55
5	3.07	3.46	1.44
10	1.44	4.28	2.84
15	1.53	4.23	2.68
20	1.34	4.33	3.05
25	1.78	4.11	2.35
30	1.62	4.19	2.55

Table 3.18

Adsorption kinetic parameters (Liquid film diffusion model) for the adsorption of Pb^{2+} on Cell-X-ZWC.

Metal ion	R^2	K_{df}
Pb^{2+}	0.49	0.07

Table 3.19

Thermodynamic value for Van't Hoff plots.

Temperature (℃)	**$[Pb]^{2+}$ (ppm) C_e**	**1/T*1000 (K^{-1})**	**lnK_d**
15	1.42	3.47	1.16
20	1.19	3.41	1.34
25	1.28	3.35	1.27
45	2.47	3.14	0.61

Table 3.20

The Pb^{2+} adsorption on polymer thermodynamic parameters.

Metal ion	**Temp.(K)**	**ΔG° (KJ/mol)**	**ΔH° (KJ/mol)**	**ΔS° (KJ/mol.K)**
Pb^{2+}	288.15	-3.24	-16.92	-0.05
	293.15	-2.99		
	298.15	-2.76		
	318.15	-1.81		

Table 3.21

ICP-MS analysis results for toxic metal concentrations in the cell-X-ZWC polymer.

Analyte	Conc. Before (ppm)	Conc. Mean (ppm)	% Adsorption
Ag	13.12	0.29	97.77%
Al	1735.63	166.77	90.39%
As	5.72	2.38	58.39%
Ba	97.4	40.55	58.37%
Be	0.30	0.013	95.68%
Bi	15.15	1.06	93.03%
Ca	165944.43	84744.55	48.93%
Cd	0.59	0.054	90.85%
Co	2.92	1.77	39.51%
Cr	1677.39	341.05	79.67%
Cu	88.37	11.01	87.54%
Fe	1902.94	363.59	80.89%
Ga	2.33	0.70	69.83%
Mn	135.07	68.63	49.19%
Mo	7.31	2.93	59.94%
Ni	17.98	10.38	42.26%
Pb	13.25	1.97	85.17%
Se	3.98	2.82	29.20%
Sr	810.59	637.77	21.32%
Te	2.23	0.41	81.85%
U	1.68	0.45	73.25%
Zn	235.48	26.18	88.88%

Appendix B

Figures

Figure 3.6

(a) Effect of initial concentration of adsorbate on the Adsorption percentage of Pb^{2+}, (b) Effect of initial adsorbate concentration on the adsorption capacity of Pb^{2+}.

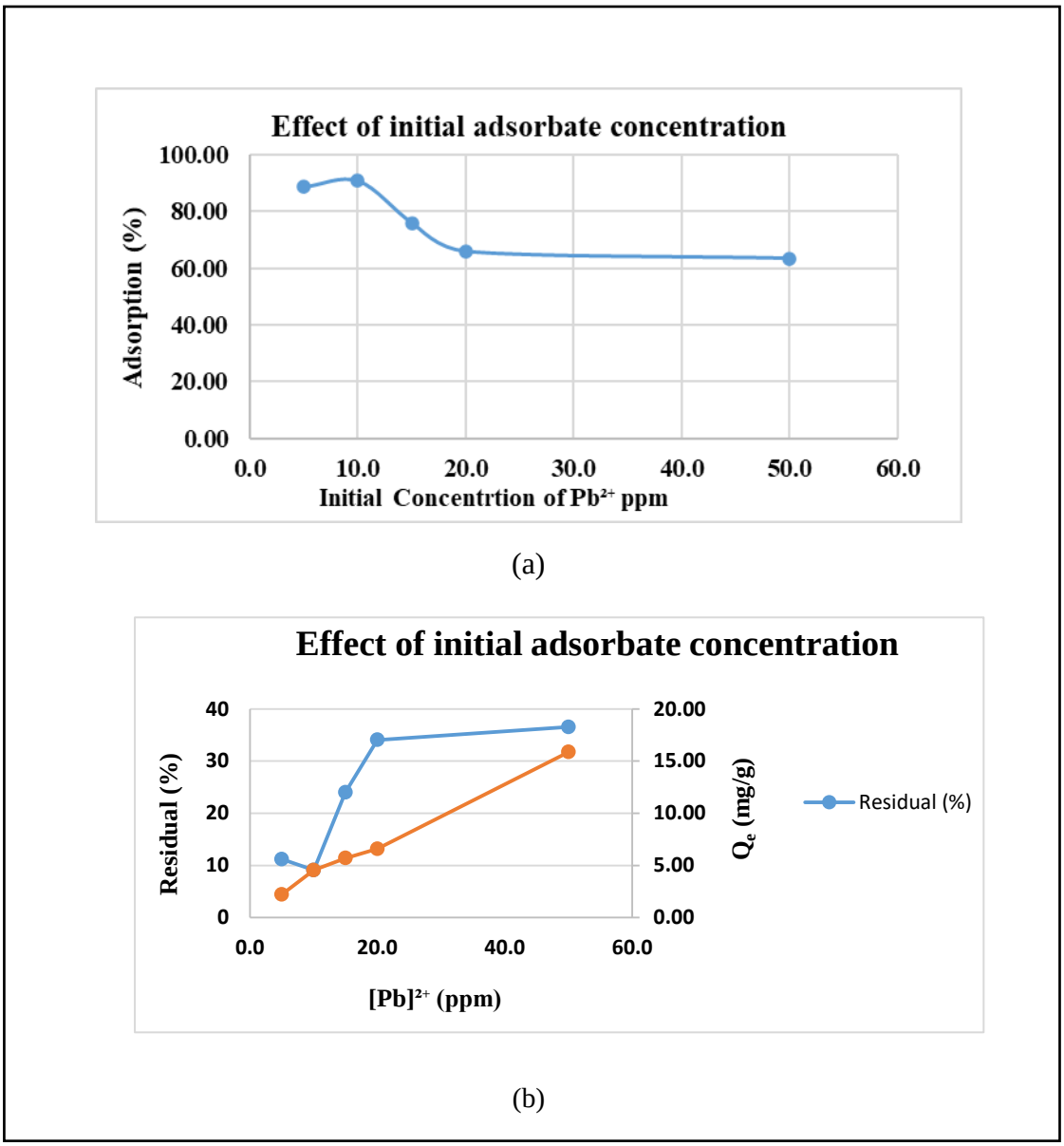

Figure 3.7

(a) Effect of contact time on the %Adsorption of Pb^{2+}, (b) Effect of contact time on the adsorption capacity of Pb^{2+}.

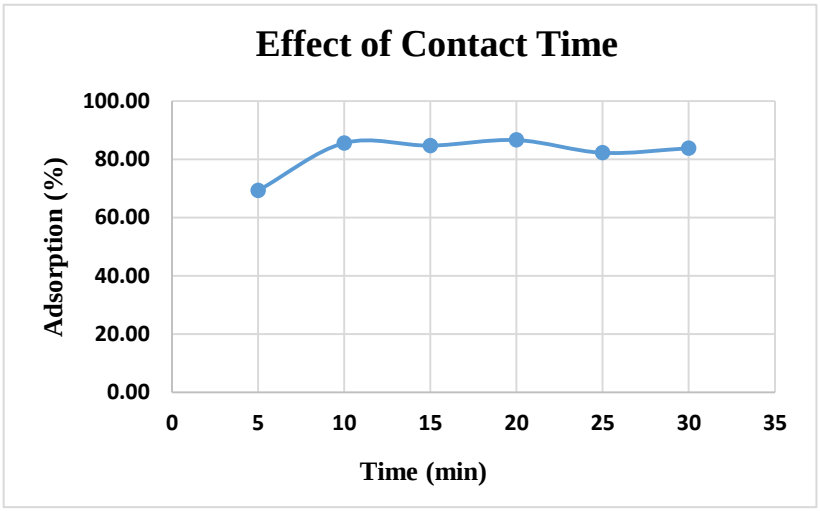

(a)

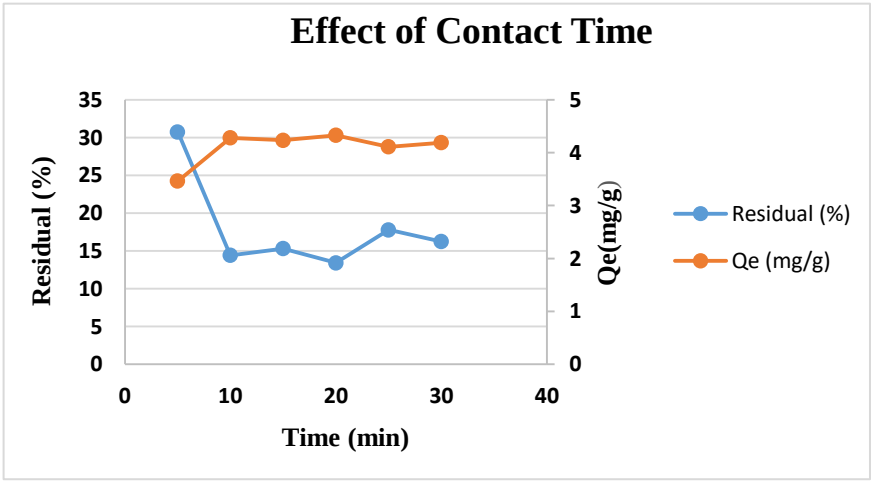

(b)

Figure 3.8

(a) Effect of adsorbent dose on %removal of Pb^{2+}, (b) Effect of adsorbent dose on %removal on the adsorption capacity of Pb^{2+}.

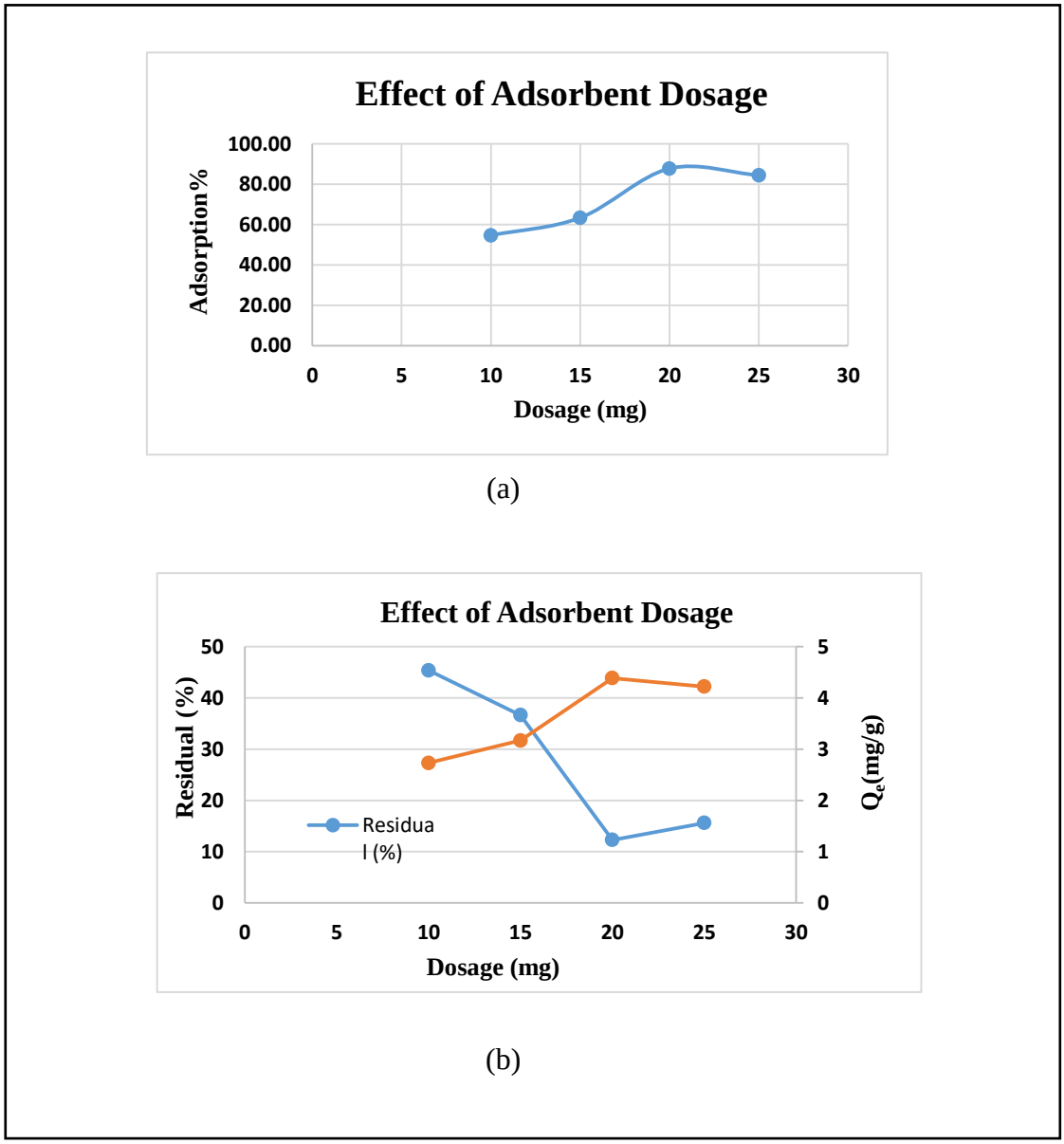

Figure 3.9

(a) Effect of Temperature on the %removal of Pb^{2+}, (b) Effect of temperature on the removal capacity of Pb^{2+}.

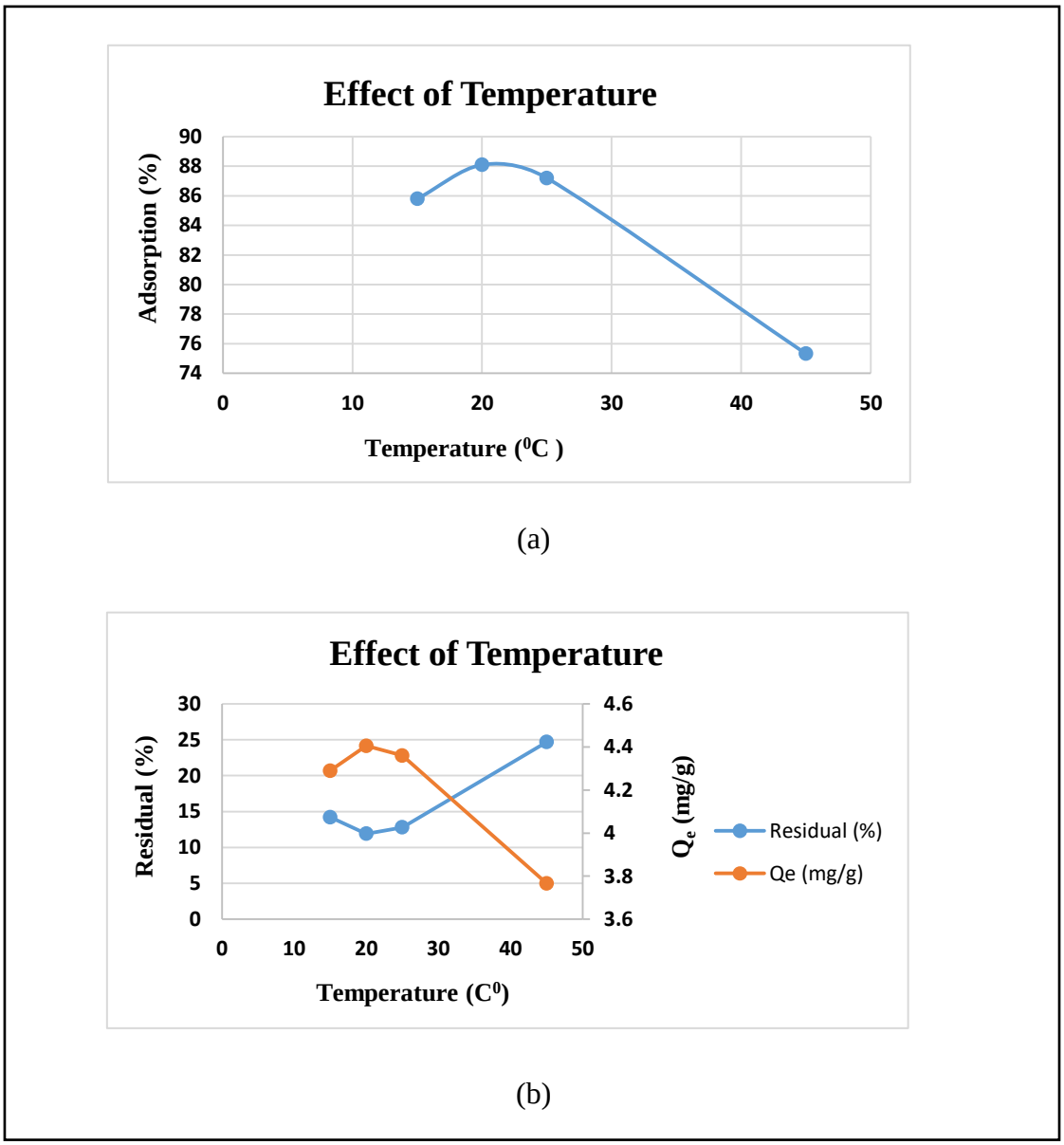

Figure 3.10

(a) Effect of pH on the %removal of Pb^{2+} ions, (b) Effect of pH on % capacity of Pb^{2+}.

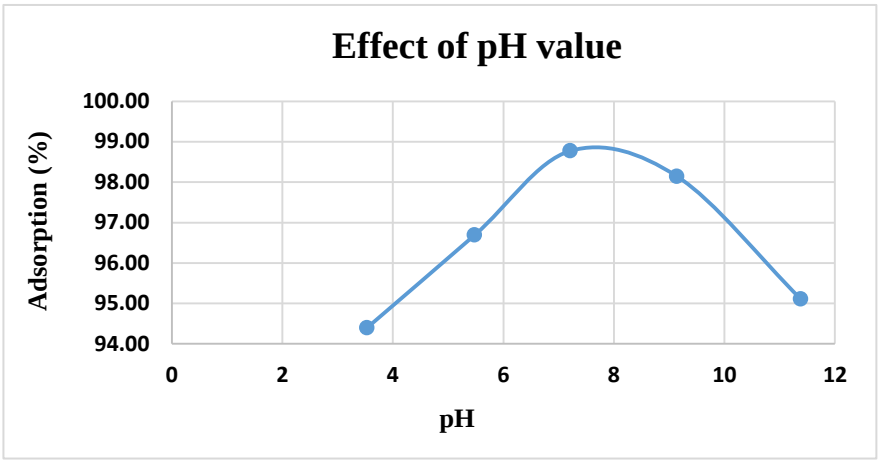

(a)

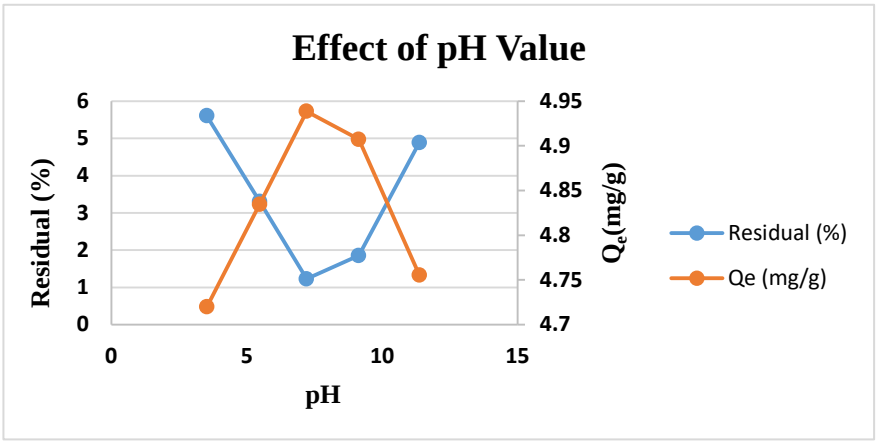

(b)

Figure 3.11

Langmuir model for adsorption of Pb^{2+} on Cell-X-ZWC.

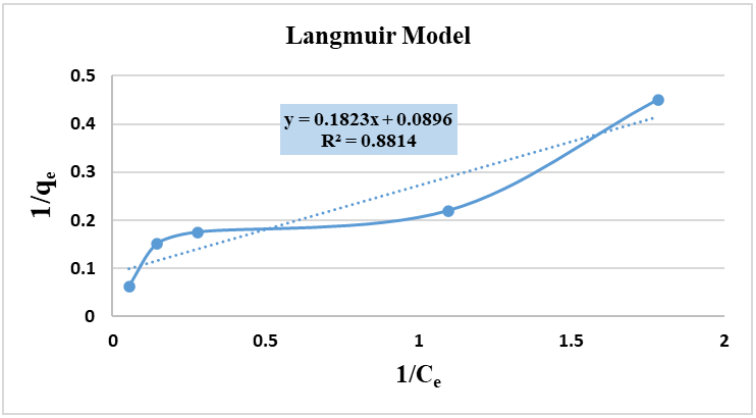

Figure 3.12

Freundlich model for adsorption of Pb^{2+} by Cell-X-ZWC.

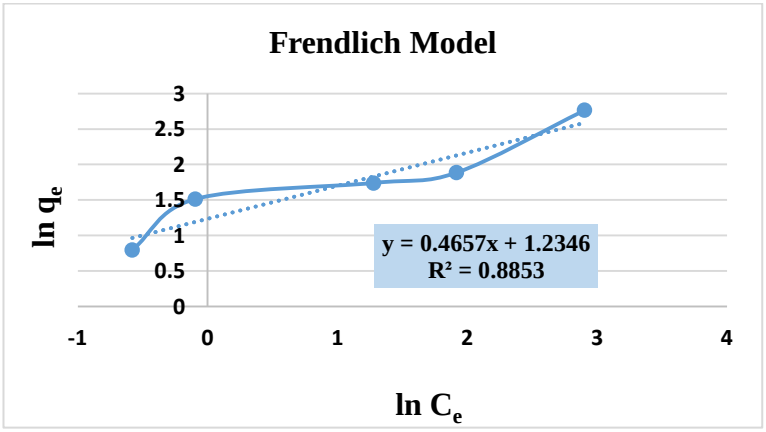

Figure 3.13

Model of pseudo-first order for Pb^{2+} absorption on Cell-X-ZWC.

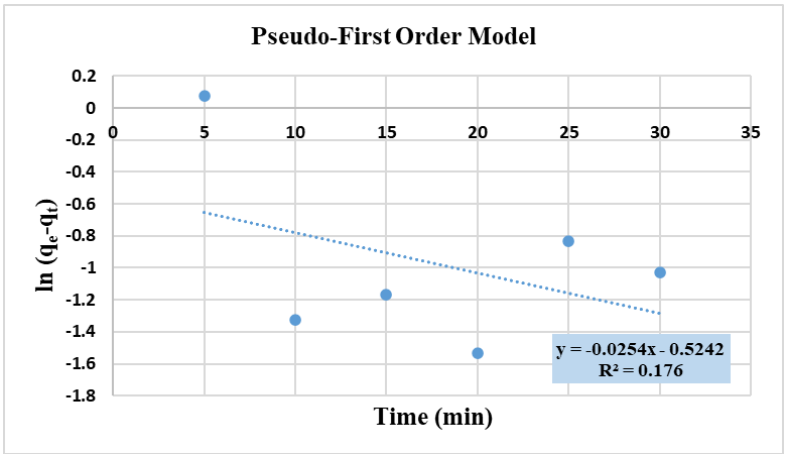

Figure 3.14

Pb^{2+} absorption on Cell-X-ZWC: pseudo-second order model.

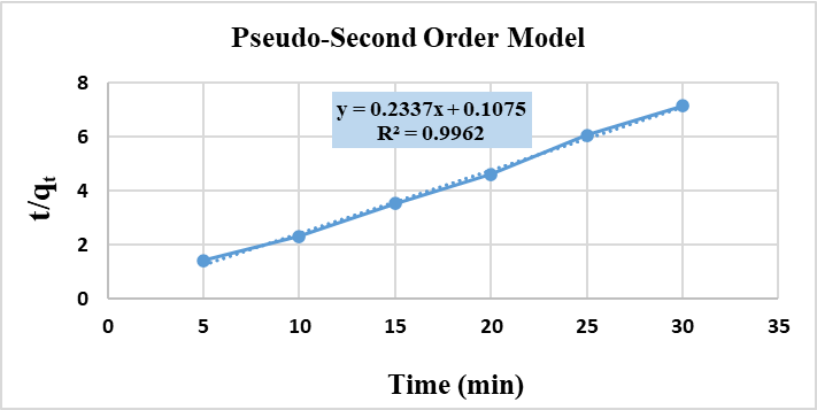

Figure 3.15

Intraparticle diffusion model of Pb^{2+} adsorption by Cell-X-ZWC.

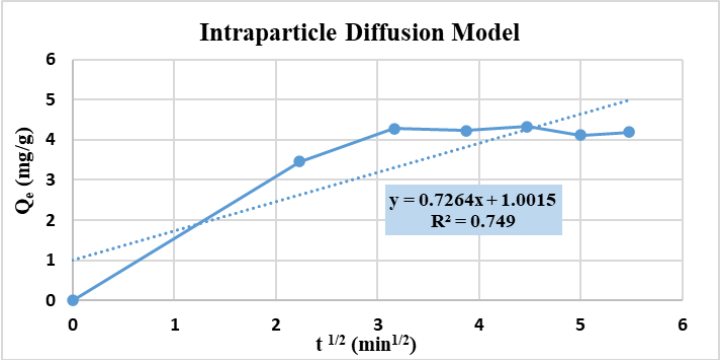

Figure 3.16

Model for the liquid film diffusion of Pb^{2+} adsorption on Cell-X-ZWC.

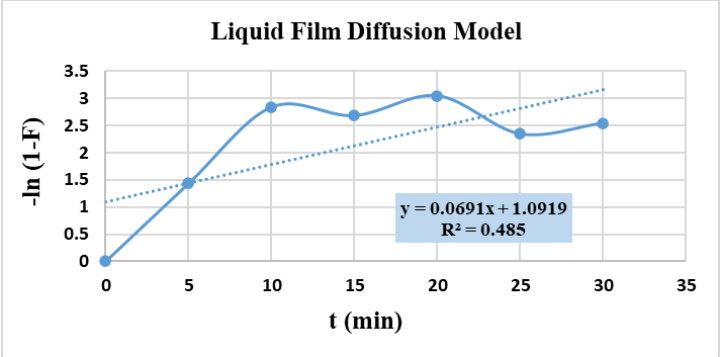

Figure 3.17

Van't Hoff diagram showing Pb^{2+} adsorption on Cell-X-ZWC.

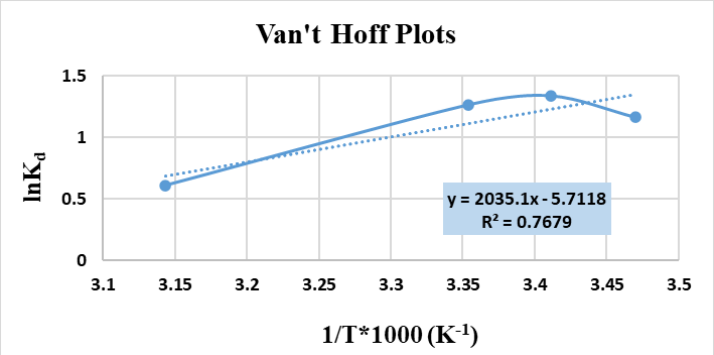

جـامعـــة النجاح الوطنية

كليـــة الدراســـات العليـــا

بوليمر مع مواقع امتزاز مزدوجة: التصميم، التركيب، والتنقية للمياه الملوثة من المعادن الثقيلة والأنيونات السامة

إعداد

رنيم أحمد "محمد رجب" أبو عايشة

إشراف

أ.د. عثمان حامد

قدمت هذه الرسالة استكمالا لمتطلبات الحصول على درجه الماجستير في الكيمياء، من كلية الدراسات العليا، في جامعة النجاح الوطنية، نابلس– فلسطين.

2023

بوليمر مع موقع امتزاز مزدوجة: التصميم، التركيب، والتنقية للمياه الملوثة من المعادن الثقيلة والأنيونات السامة

اعداد

رنيم أحمد "محمد رجب" أبو عايشة

اشراف

أ.د.عثمان حامد

الملخص

الطلب على النظافة آخذ في الازدياد بسبب الزيادة في عدد السكان. إعادة تدوير مياه الصرف الملوثة يمكن أن تكون حلاً لهذه المشكلة. مياه الصرف ملوثة بمجموعة متنوعة من المواد السامة حسب مصدر التلوث. الملوثات تشمل بشكل أساسي أيونات المعادن والمواد العضوية التي يتم إطلاقها من مصادر مختلفة منها الطبية والزراعية والسباكة والمواد الكيميائية المنزلية ومنتجات العناية بالجسم والصناعات. من بين أيونات المعادن الثقيلة السامة التي تثير القلق الشديد هي Cr^{2+}, Cd^{2+}, Hg^{2+}, Pb^{2+} وغيرها من المعادن التي تضر بالمخلوقات. لإزالة الملوثات الخطرة من المعادن الثقيلة و لتحسين جودة المياه ، استخدم الباحثون العديد من الممتزات التي تعتمد على البوليمر. يمكن أن يكون تعديل البوليمرات الموجودة هو أبسط طريقة وأكثرها فعالية لتوليد مادة ماصة منخفضة التكلفة ذات كفاءة عالية لإزالة المعادن والمركبات العضوية الخطرة.

تم التخطيط لهذا العمل لتحضير السليلوز مع مواقع تنسيق متعددة ومجموعات وظيفية من الأيونات المزدوجة. هذه المعايير تجعله متفوقًا في الامتصاص لاستخدامه في تنقية مياه الصرف الصحي الملوثة.

تم تصميم السليلوز المستهدف ليكون لديه مواقع ارتباط للمعادن الثقيلة السامة والأنيونات السامة مثل النترات. طريقة تحضير البوليمر تتكون من ثلاث خطوات:تتضمن الخطوة الأولى إضافة الألدهايد كمجموعة وظيفية إلى مسحوق السليلوز عن طريق الأكسدة (سيليلوز– ألدهايد). في الخطوة الثانية تم ربط (سيليلوز–ألدهايد) بعديد الأمين مثل بارا–فينيلين داي أمين لإنتاج شكل ثلاثي الابعاد مع مواقع تنسيق متعددة، والذي سيتفاعل بعد ذلك مع

1,4–بيوتان سلتون لتشكيل بوليمر السيليوز المستهدف مع مجموعات وظيفية من الأيونات المزدوجة. تم تأكيد بنية البوليمر بواسطةالتحليل الطيفي للأشعة تحت الحمراء.

تم تقييم البوليمر لقدرته على امتصاص أيونات الرصاص. تمت دراسة كفاءة الامتزاز كدالة لدرجة الحرارة، درجة الحموضة ، وقت التلامس ، الجرعة وتركيز أيونات المعادن. الكفاءة العالية في امتصاص المعادن الثقيلة من مياه الصرف الصحي ، مع أقصى نتيجة امتزاز لـ Pb^{2+} تبلغ 97.43٪ عند الرقم الهيدروجيني 7.21 ، ووزن الجرعة = 20 ملغم ، والتركيز الأولي لأيون المعدن = 10 جزء في المليون ، والوقت = 20 دقيقة ودرجة الحرارة 20 درجة مئوية. لفهم تلقائية وآلية الامتزاز ، تمت دراسة متساوي الامتزاز ، وعلم الحركة ، والديناميكا الحرارية. المعلمات الديناميكية الحرارية لامتزاز أيونات الرصاص تلقائي ($\Delta G°<0$)، طارد للحرارة ($\Delta H°<0$)، يحدث التفاعل تلقائياً في درجات حرارة منخفضة ($\Delta S° <0$). تتبع جميع عمليات الامتزاز نموذج حركية الامتزاز من الدرجة الثانية ($R^2 = 0.99$)، والذي تم إنشاؤه بواسطة معلمات الامتزاز ، وقد تمت مطابقة هذه الامتزازات مع متساوي درجة حرارة فروندليتش للامتزاز ($R^2 = 0.89$).

تم تحضير المركب المستهدف وتحديده بواسطة التحليل الطيفي للأشعة تحت الحمراء، لديه استقرار حراري جيد ، وعليه فهو يمتص المعادن من مياه الصرف بكفاءة عالية.

الكلمات المفتاحية: السليلوز ، تلوث المياه ، معالجة مياه الصرف الصحي ، المعادن الثقيلة ، الرصاص، بارا–فينيلين داي أمين، 1,4–بيوتان سُلتون، أيون مزدوج.